



VILNIUS GEDIMINAS TECHNICAL UNIVERSITY
FACULTY OF ELECTRONICS
DEPARTMENT OF AUTOMATION

Darío Delgado Esteban

HEXAPOD ROBOT STABILITY RESEARCH

Final Bachelor Thesis

Automation and control studies program, National code 612H62002

Kompiuterinio technologijų valdymo specializacija

Electrical and Electronic engineering studies course

Vilnius, 2015



VILNIUS GEDIMINAS TECHNICAL UNIVERISTY

ELECTRONICS FACULTY
DEPARTMENT OF AUTOMATION

ASSERT
Department head

(Signature)

Name: assoc. prof. dr. Zita Savickienė

2015 y. _____ m. ____ d.

Darío Delgado Esteban

HEXAPOD ROBOT STABILITY RESEARCH

Final bachelor thesis

Automation studies program, National code 612H62002

Kompiuterinio technologijų valdymo specializacija

Electrical and Electronic engineering studies course

Supervisor assist. Mindaugas Luneckas
(Sci. degree, name, surname)

(Signature)

(Date)

Consultant doc. dr. Tomas Luneckas
(Sci. degree, name, surname)

(Signature)

(Date)

Vilnius, 2015



Vilnius Gediminas Technical University

Faculty of electronics

Department of Automation

ISBN

Copies No...

Date 20-01-2015

Bachelor Degree Studies **Automation** study programme Bachelor Graduation Thesis 3.

Title: **Hexapod robot stability research.**

Author: **Darío Delgado Esteban**

Academic supervisor: **Assist. Mindaugas Luneckas**

Thesis Language: English

Annotation

In this final thesis, a method for designing a new body for a hexapod robot is proposed, in which the optimization of its stability is the main purpose. Several designs are discussed, analyzing their advantages and disadvantages and also calculating the optimum parameters for maximum stability. The most suitable design is proposed to be built.

Work size: 58 pages of text, 25 figures, 14 tables.

Key words

Hexapod robot, static stability, dynamic stability, legged robot, gaits.



Vilniaus Gedimino technikos universitetas

ISBN

Elektronikos fakultetas

Egz. sk.

Automatikos katedra

Data 2015-20-01

Pirmosios pakopos studijų Automatikos programos bakalauro baigiamasis darbas 3.

Pavadinimas: **Šešiakojo roboto stabilumo tyrimas.**

Autorius: **Darío Delgado Esteban**

Vadovas: **Mindaugas Luneckas**

Kalba: anglų

Anotacija

Šiame darbe tiriamas naujas metodas šešiakojo roboto kūno kurimui, atsižvelgiant į statinį ir dinaminį stabilumą. Aptariami keli skirtingi pagrindinio roboto kūno variantai, jų privalumai ir trūkumai. Taip pat yra skaičiuojami optimaliausi parametrai, kad pasiekti maksimalų stabilumą. Atsižvelgiant į visus kriterijus yra siūlomas tinkamiausias kūnas.

Darbo dydis: 58 puslapiai, 25 paveikslai, 14 lentelių.

Prasminiai žodžiai

Šešiakojis robotas, statinis stabilumas, dinaminis stabilumas, vaikščiojantis robotas, eisenos.



VILNIUS GEDIMINAS TECHNICAL UNIVERSITY

Dario Delgado Esteban, 20147902

(Student's given name, family name, certificate number)

Faculty of Electronics

(Faculty)

Automation, ATVf-11

(Study programme, academic group no.)

**DECLARATION OF AUTHORSHIP
IN THE FINAL DEGREE PROJECT**

January 20, 2015

I declare that my Final Degree Project entitled „Hexapod robot stability research“ is entirely my own work. The title was confirmed on November 21, 2014 by Faculty Dean's order No. 235 el. I have clearly signaled the presence of quoted or paraphrased material and referenced all sources.

I have acknowledge appropriately any assistance I have received by the following professionals/advisers: Mindaugas Luneckas, Tomas Luneckas.

The academic supervisor of my Final Degree Project is Mindaugas Luneckas.

No contribution of any other person was obtained, nor did I buy my Final Degree Project.

Dario Delgado Esteban

(Signature)

(Given name, family name)



INDEX

INTRODUCTION	8
Legged locomotion	9
Applications of legged vehicles	9
Objective	10
1. ANALYTICAL PART	11
1.1. Robot Body Architecture	12
1.2. Design of the legs	13
1.2.1. Architectures of Legs	13
1.2.2. Leg frame and notations.....	14
1.2.3. Robot Leg Parameters.....	14
1.2.5. Inverse Kinematics.....	15
1.3. Actuators arrangements	16
1.3.1. Servos.....	17
1.4. Movement of the robot. Gaits	19
1.5. What is stability?	22
1.5.1. Energy stability margin, ESM.....	25
1.5.2. Normalized Energy Stability Margin, NESM.....	25
1.5.3. Dynamic stability margin, DSM	26
1.5.4. Force-Angle Stability Margin, FASM	26
1.5.5. Normalized Dynamic Stability Margin, NDSM	27
1.6. Analysis of relationship between stability margin and dexterity	30
1.7. Terminology	32
2. DEVELOPMENT OF THE ROBOT.....	33
2.1. Design Considerations	33
2.2. Modeling	34
2.2.1. Leg structure	34
2.2.2. Design of the body	34
2.2.3. Displacement of the middle legs	36
2.2.4. Offset in the coxa angle in front and rear legs	39
2.2.5. Models.....	39
2.2.6. Design of the leg disposition and step length.....	40



2.3. Check static stability in transfer phase 45
 2.3.1. Static Stability Checking Procedure 46
2.4. Model to be constructed 47
 2.5.2. Body tilt 50
 2.5.3. Y-Sway Motion..... 51
 2.5.4. E-Sway Motion 51
3. CONCLUSIONS..... 53
4. REFERENCES 54
ANNEX I 56



INTRODUCTION

It is clear that nowadays the technology has become a part of our lives. Since the first semiconductor material was developed, the evolution of electronics has led a revolution that nobody knows how far can go. Not only our quality of life has been improved; safer activities in factories, the ability of producing better and faster, travelling to unknown places, or even exploring the space. These are some examples in which the humanity has taken advantage of the electronic and automotive devices.

One of the most important achievements of humanity in this field was to create a machine called robot. It is well known that this machine could have many definitions, but the one accepted all over the world could be:

*“A **robot** is a mechanical or virtual artificial agent, usually an electro-mechanical machine that is guided by a computer program or electronic circuitry. Robots can be autonomous or semi-autonomous and range from humanoids to industrial robots, collectively programmed 'swarm' robots, and even microscopic nano-robots”* [1].

In fact there are now so many kinds and types of robots that given a generic description for all of them may be not descriptive enough. But there is one kind of robot that in the recent twenty years has increased its popularity. It is not other than the autonomous robot:

*“An **autonomous robot** is a robot that performs behaviors or tasks with a high degree of autonomy, which is particularly desirable in fields such as space exploration, cleaning floors, mowing lawns, waste water treatment and delivering goods and services.”* [2].

The first prototypes made have a common fact, which is that the designer tried to imitate the nature, either animals or human being. Although many animals in nature have legs for locomotion, the very first vehicles developed by human have been with wheels. Following the invention of the steam engine and widespread use of the railways, and then the development of the combustion engines, wheeled locomotion has become the most widespread technology of transportation. Despite its success on predetermined and plane surfaces, wheeled locomotion is not proper for unknown and rough terrains. The tracked (palette) locomotion is developed in order to cope with this problem. However, tracked locomotion is also problematic, since it destroys the terrain on which the vehicle is moving. As an alternative to both wheeled and tracked forms, legged locomotion is developed by imitating the legged animals in nature [3].

The aim of this final thesis is to study the stability of a hexapod robot. A discussion about the parameters and different methods of measuring the stability is firstly proposed. Then a discussion about the best body configuration and leg disposition is shown, always trying to develop the maximum stable design. Finally, the best prototype is proposed to be constructed.



Legged locomotion

From what was seen, it is possible to conclude that legged locomotion vehicles present a superior mobility in natural terrains, since these vehicles may use discrete footholds for each foot, in opposition to wheeled vehicles, that need a continuous support surface. Therefore, these vehicles may move in irregular terrains, by varying their legs configuration in order to adapt themselves to surface irregularities and, on the other way, the feet may establish contact with the ground in selected points in accordance with the terrain conditions. For these reasons, legs are inherently adequate systems for locomotion in irregular ground [4]. The use of multiple degrees of freedom in the leg joints, allows legged vehicles to change their heading without slippage. It is also possible to vary the body height, introducing a damping a decoupling effect between terrain irregularities and the vehicle body [5].

Another advantage that is recently being investigated, concerns failure tolerance during static stable locomotion. The consequence of a failure in one of the wheels of a wheeled vehicle is a severe loss of mobility, since all wheels of these kinds of vehicles should be in permanent contact with the ground during locomotion. However, legged vehicles may present a redundant number of legs and, therefore, can maintain static balance and continue its locomotion even with one or more of its legs damaged [6].

Last, it should be mentioned that legs can be used not only for locomotion purposes, but also with the vehicle in static position. For instance, the body can be actively actuated while feet are fixed to the ground, working as an active support base for helping the motion of a manipulator mounted on the body [7]. As an alternative to the assembly of a manipulator on the robot body, multilegged robots can use one or more of its legs to manipulate objects, as it is possible to see in some animals (several animals use their legs to hold, manipulate and transport objects).

Applications of legged vehicles

Mobile robots, independently of its locomotion principle, are adequate for 3-D environments (Dirty, Doll, Dangerous). These vehicles are able to replace human beings, in order to avoid danger to their lives, in all kinds of dangerous works that require heavy safety measures or in areas to which the humans cannot easily access.

In case of legged locomotion robots, examples of these situations are [8]:

- Remote locations exploration:
 - In volcanoes (*“Dante II”*, by the Carnegie Mellon team, led by Dr. William L. Whittaker and Dr. John E. Bares).
 - In space or other planets (*“ATHLETE (All-Terrain Hex-Legged Extra-Terrestrial Explorer)”* by the Jet Propulsion Laboratory (JPL) at California Institute of Technology).
 - In the bottom of the sea (*“Crabster CR2000b”*, by the Korean Institute of Ocean Science and Technology (KIOST)).



- Hostile or dangerous environments:
 - In nuclear power plants or in places with high radiation levels (*“Quadruped walking robot” by Toshiba, used in Fukushima Daiichi nuclear power plant*).
 - In disaster areas or catastrophe situations (*“COMET-I” by Chiba University, Japan*).
 - In search and rescue operations (*“Cheetah-cub robot”, by the Swiss Federal Institute of Technology (EPFL)*).
 - In military operations (*“BigDog”, by DARPA*).

Besides these applications, legged robots can also be used in a large variety of tasks such as:

- In excavation and construction works (*“MELMALEC”, by Mechanical Engineering Laboratory, AIST, MITI, Japan*).
- In helping humans during payload transport operations (*“QU 1120”, by HTR*).
- In services, especially for maintenance of pipes and narrow spaces (*“RHex”, by BostonDynamics*).

It is obvious that this type of robots can suit in a wide range of applications. Generally speaking, however, walking robots have many shortcomings that bar them from wider use in industry and services. For instance, legged robots are still heavy, bulky, very slow and inefficient from the energy expenditure point of view, which is a fundamental issue in autonomous robots. In other words, although legged robots have already demonstrated their capability to perform many tasks wheeled or tracked vehicles cannot handle, some features must still be improved before legged robots can meet present requirements in industry and services. In this work it will be shown a method to improve the stability of a six legged robot, which main aim is not commercial, only to understand its behavior.

Objective

“Develop a body configuration for a hexapod robot maximizing its stability”

1. ANALYTICAL PART

When we start from zero a new project, we should have in mind every possibility of design and try to get rid of the designs that are not suitable for our goal. Nowadays is difficult to find a configuration that has not been tested already. Research on legged locomotion has a long history. Biologists and other scientists have long studied the structure and motion of animals. Basically, every project of legged robot started from the same idea of imitating the nature of animals and human being and the biomechanics implicated.

In the next picture we can see a basic scheme of the possibilities of configurations for hexapods [9]:

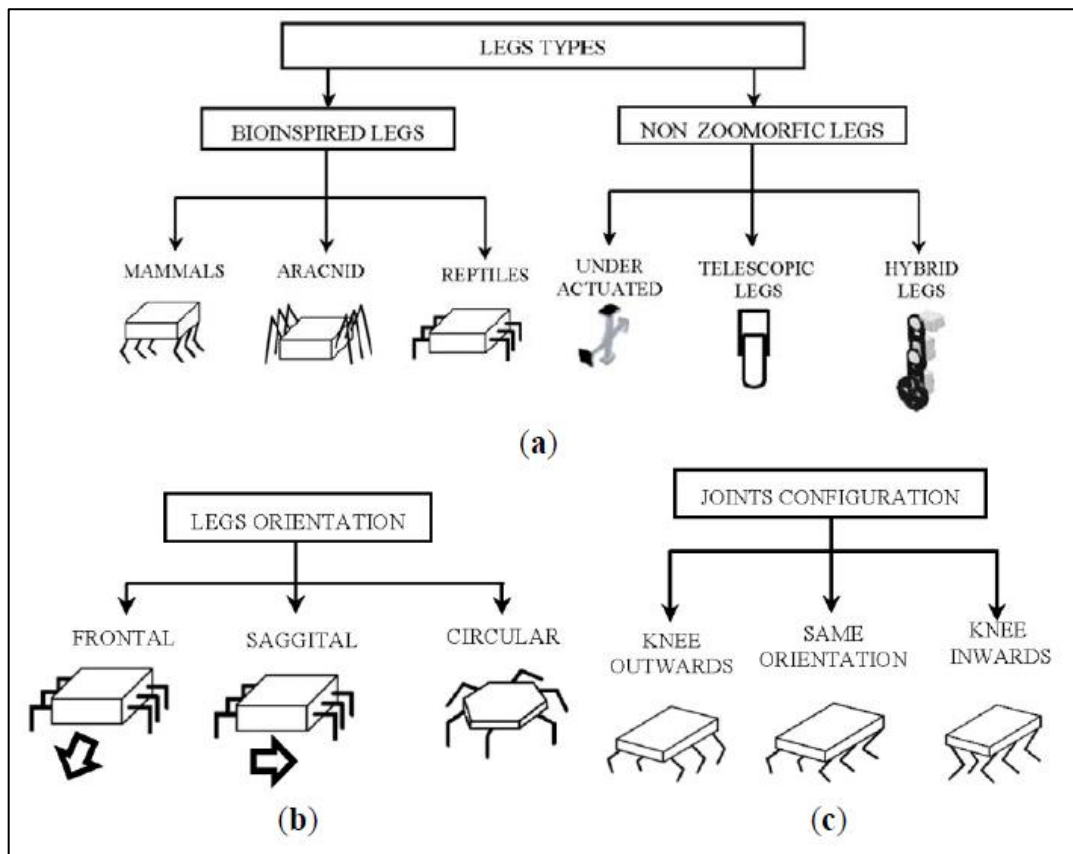


Figure 1. Type setting of hexapod legs' design [9].

1.1. Robot Body Architecture

There are two basic architectures of hexapod robots: **rectangular** and **hexagonal**. The first one has six legs distributed symmetrically along two sides, each side having three legs. The second has legs distributed axi-symmetrically around the body, in a hexagonal or circular shape. Many references can be found in the literature on rectangular six-legged robots. In paper [10], Lee et al. describe the longitudinal stability margin for rectangular hexapods. Also, the feasible walking gaits have been widely investigated and tested. Bilateral symmetry may be better suited than radial symmetry to move along a straight line. Rectangular architectures require a special gait for turning action; generally, they need four steps in order to realize a turning action [11]. Hexagonal hexapod robots demonstrate better performances than rectangular robots for some aspects. As example hexagonal robots can have many kinds of gaits and can easily change direction—in fact true radial symmetry implies that all legs are equal and the body has no “front” or “rear”—there is thus no preferential direction for the motion. In paper [12], Preumont et al., proved that hexagonal hexapods can easily steer in all directions and that they have a longer stability margin. In paper [13], Takahashi et al., found that hexagonal robots rotate and move in all directions at the same time, better than rectangular ones, by comparing stability margin and stroke in wave gait. Chu and Pang in paper [14] proved theoretically that hexagonal hexapod robots have superior stability margin, stride and turning ability compared to rectangular robots.

In the next picture we can see the the advantages of the hexagonal body against the rectangular in the turning task depending on the Q/P ratio [15]:

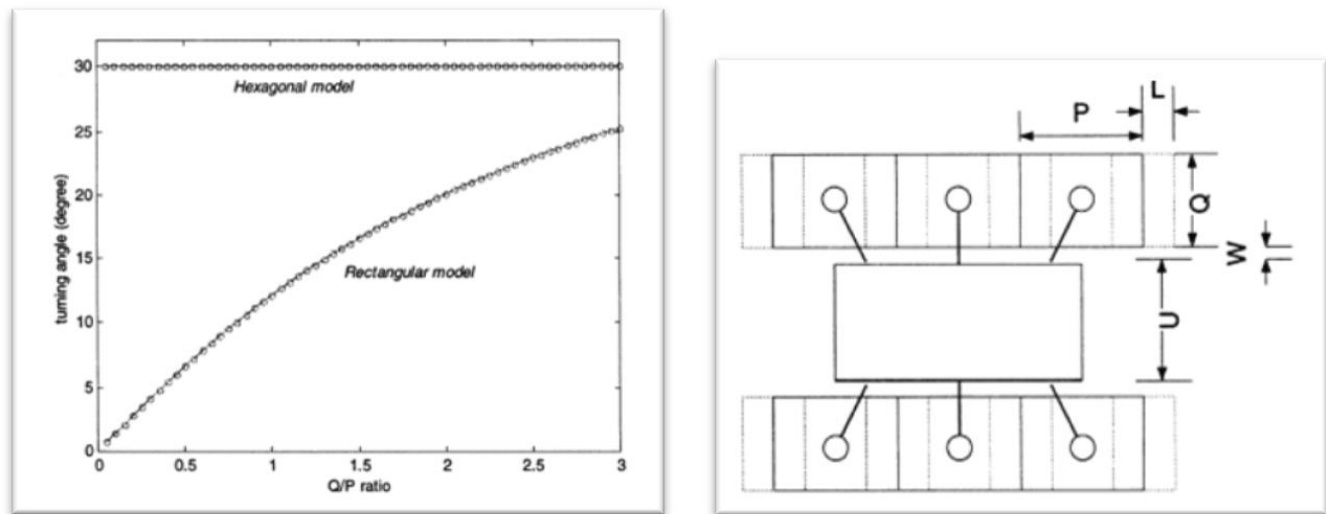


Figure 2. On the left the comparison between the G/P ratio of the Hexagonal mode against the Rectangular mode. On the right a detail of the parameters of the hexapod robot [35].

As a way of summarize, we would say that the hexagonal architecture has advantages in turning gait while rectangular has advantages in straight forward gait. It is clear that assuming the same leg design and robot size, the hexagonal model shows better turning ability, higher stability margin and greater stride length in certain conditions.

Nevertheless, as our intention is to take advance of the old robot and all its software developed, we will take the design of the rectangular hexapod. The next step in the improvement of the design will be the understanding of all the parameters involved on the movement of the robot and a deep search on the methods that could set a better stability for the robot.

1.2. Design of the legs

1.2.1. Architectures of Legs

Kinematics architecture depends on the factors related to the application in which the hexapod robot is required for, as for example the terrain's form, the workspace, and the payload. Literature shows that there is a number of different leg types currently employed for hexapod walking robots. All have advantages and disadvantages. Fig. 1(a) shows a schematic classification of hexapod legs types.

At the first stage, one can choose between bio inspired and non-zoomorphic legs. Bio inspired leg configuration is motivated primarily by animal gait, such as reptiles, mammals or arachnid. The first one has legs and bodies for moving over rough and uneven terrains [17]. The principal characteristic of the Reptilian type is that the legs are placed on both ends of the protruding body and knees to the side of the base. Mammals' bodies are above the legs, which gives less support to the base and lower power consumption is needed to support the body, but it requires more stability than other types of animals [18]. In arachnid configuration, leg's extremities are situated on both sides, sticking the knees at the top of the spider's body. The orientation of the legs in respect to the body of the hexapod robot can be done with three configurations (Fig. 1(b)): frontal, sagittal or circular. In the first one, the directions are perpendicular to the advancement of the legs' position, unlike the sagittal, which moves parallel to the robot legs, while in the circular arrangement the legs are positioned radially to the body of the system allowing the mechanism to move in any direction [19]. In the mammalian configuration, the legs are below the body and can place the knees in different positions depending on the application it requires (Fig. 1(c)). Non zoomorphic legs can be hybrids such as in paper [20], telescopic such as in paper [22], or under-actuated such as in paper [23]. In paper [21], a solution named Roller-Walker is presented. The principle through which the robot propels itself during wheeled locomotion is the same as that of the skaters.

1.2.2. Leg frame and notations

The coordinate frames for the robot legs are assigned as shown in Fig. 3. The assignment of link frames follows the Denavit-Hartenberg notation. The robot leg is made of links and joints; different links of robot leg are called Coxa or Hip, Femur and Tarsus. Those names are given by the bones of human leg. The robot leg frame starts with link 0 which is the point where the leg is attached to the body, link 1 is Coxa, link 2 is the Femur and link 3 is Tibia. The joints are located at the inner end of their respective link frames are attached to outer end of their respective links.

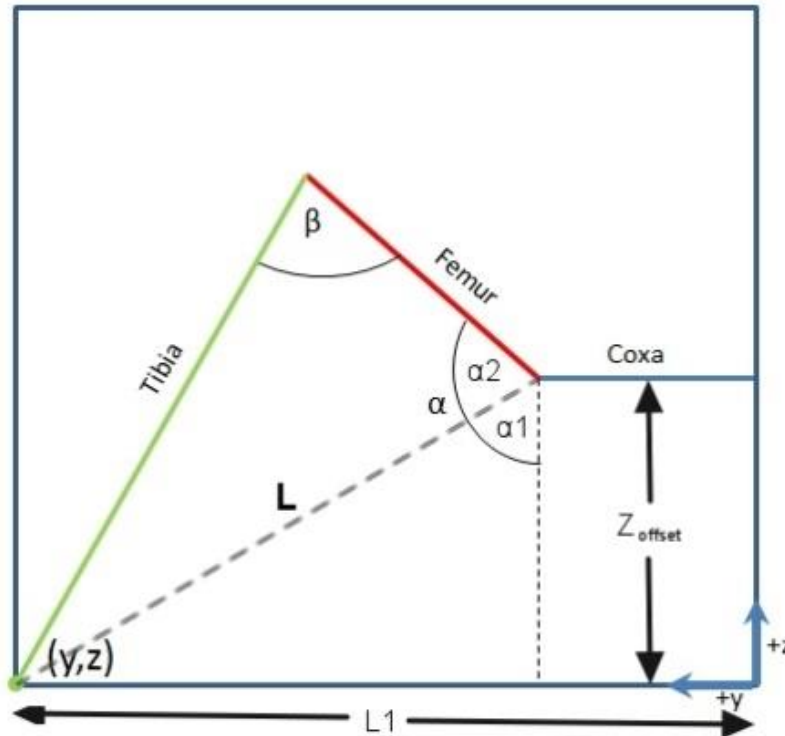


Figure 3. Different parts of the hexapod's leg [36].

1.2.3. Robot Leg Parameters

The kinematic model here is derived by defining the reference frames according to the Denavit-Hartenberg convention. In Fig. 3 graphical representation of a three joint robot leg is given, with the attached reference frames and corresponding joint variables. In order to obtain the position of the robot's foot knowing the angles of the three joints, and the other way around, which is the angles of the joints knowing the foot position, we will use the well-known algorithm of Denavit-Hartenberg in Forward kinematics and in Inverse kinematics respectively.

1.2.4. Forward kinematics

Forward kinematics refers to the use of the kinematic equations of a robot to compute the position of the end-effector from specified values for the joint parameters. In this case, the end effector is considered to be the end of the robot's leg.

From leg kinematic layout showed in Fig. 4, Denavit-Hartenberg solution gives the following three equations:

$$\begin{aligned} x &= \cos\theta_1 \cos\theta_2 l_3 \cos\theta_3 - \cos\theta_1 \sin\theta_2 l_3 \sin\theta_3 + \cos\theta_1 l_2 \cos\theta_2 \\ y &= \sin\theta_1 \cos\theta_2 l_3 \cos\theta_3 - \sin\theta_1 \sin\theta_2 l_3 \sin\theta_3 + \sin\theta_1 l_2 \cos\theta_2 \\ z &= -\sin\theta_2 l_3 \cos\theta_3 - \cos\theta_2 l_3 \sin\theta_3 - l_2 \sin\theta_2 \end{aligned} \quad (1)$$

These equations provide a relation between the positions of robot's feet and the angle of the servos used as actuators. As it can be observed, they provide the foot position when these angles are known, which means forward kinematics.

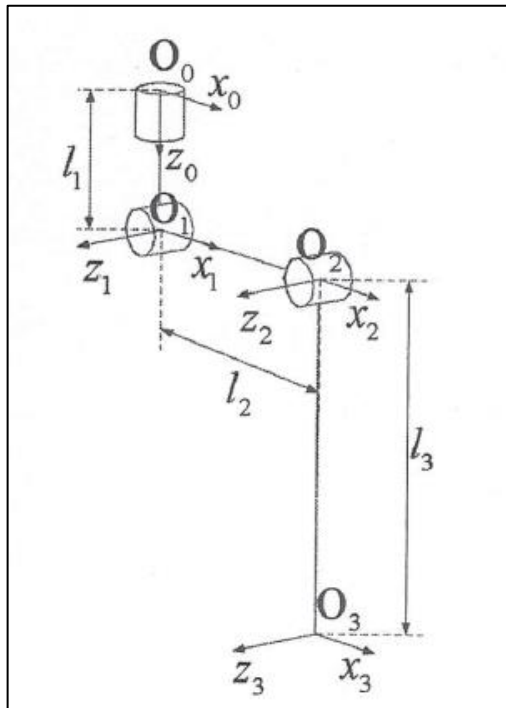


Figure 4. Similar scheme of the Denavit-Hartenberg axis and lengths [37].

1.2.5. Inverse Kinematics

In order to get inverse kinematics expressions, it is necessary to express θ_1 , θ_2 and θ_3 over x , y and z . Such task could be very complex or even unsolvable.

Less complex way of dealing with robot's inverse kinematics is geometric inverse kinematics method. The following figures demonstrate kinematic layout of one leg for geometric inverse kinematics (Fig. 5) [24].

The following expressions are derived using this method:

$$\begin{aligned}
 \theta_1 &= \arctan \frac{y}{x+l_3}, \\
 \theta_2 &= q_1 + q_2, \\
 \theta_3 &= \arccos \frac{l_1^2 + l_2^2 - B}{2l_1 l_2}, \\
 l_4 &= \sqrt{x^2 + y^2} + l_3, \\
 B &= \sqrt{(l_4 - l_3)^2 + z^2}, \\
 q_1 &= \arcsin \frac{z}{B}, \\
 q_2 &= \arccos \frac{l_1^2 - l_2^2 + B}{2l_1 B}
 \end{aligned} \tag{2}$$

Where θ_1 , θ_2 and θ_3 are leg actuator angles that must be calculated in order to position robot's foot into position with coordinates x , y and z .

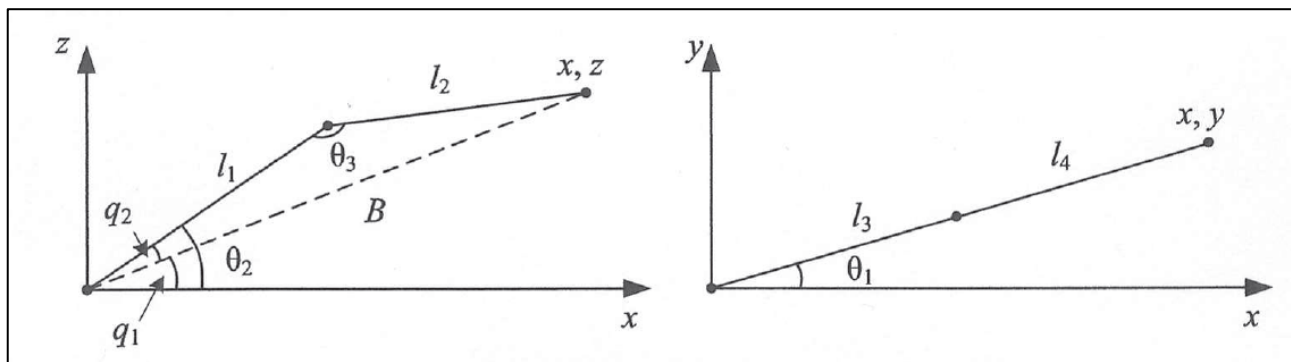


Figure 5. Leg projection onto XZ and XY planes [37].

1.3. Actuators arrangements

Typically, specific actuator arrangements are developed in order to obtain maximum leg workspace with a minimal kinematic structure. The design consists of links connected through knee joints. The walking motion is accomplished by controlling the angle of the links to position the feet. There is a number of different ways in which the joints can be actuated, which are referenced in [25].

Options include mounting the motor at the joint itself, or using a pulley and belt (Fig. 6b) or lead screw (Fig. 6c) to set the angle of the knee using an actuator mounted near the base of the leg [32].

The major drawback of last design is the necessity to actuate remote joints. On the other hand, latching the actuator at the knee joint adds various dynamic effects to the leg which have to be compensated by the controller. This adds complexity to the control algorithms needed to move the leg. It also requires more powerful motors at the hip joint to move the added mass of the leg. Remote actuation, in which the actuators are located at the base of the leg, eliminates some of these problems, at the cost of increasing the complexity of the mechanism. The coupling of the motion of the end effector relative to the actuators is another undesirable characteristic of this leg design.

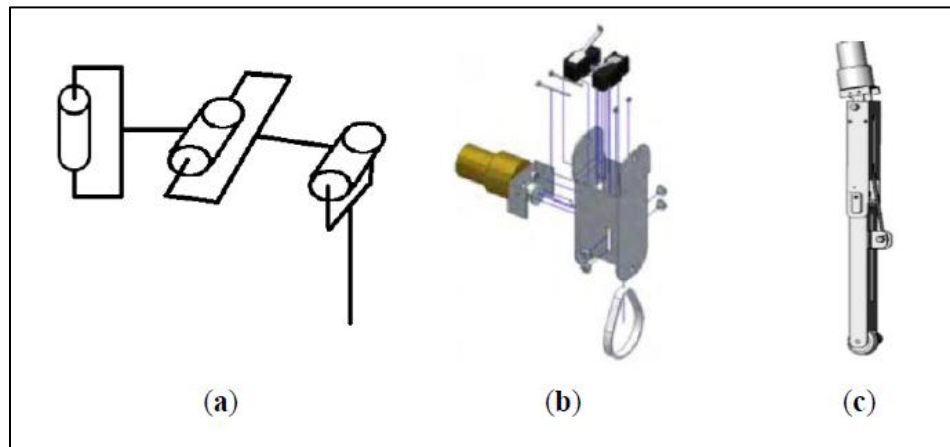


Figure 6. Different types of actuators [9].

Another potential leg design is modeled according to a typical mammalian leg with a four-bar linkage structure. The major drawback of this design is that the motions are highly coupled and the effective workspace is somewhat limited. Moreover, the entire weight of the robot is supported by the hip joint and they necessitate a powerful and expensive motor.

1.3.1. Servos

The actuators used for the hexapod are Dynamixel AX-12 servos. These actuators have been selected because of the good results given by the previous prototype, which used them for leg movement. A total number of 18 servos are necessary to obtain 3 degrees of freedom in each leg, so three of those actuators will be placed in each leg. The main characteristics and properties of the servos are showed below. For further details, the developer of this product provides a datasheet.



Table 1. Servo properties [38].

	AX-12	
Weight (g)	55	
Gear Reduction Ratio	1/254	
Input Voltage (V)	At 7V	At 10V
Final Max Holding Torque (kgf.cm)	12	16.5
Sec/60degree	0.269	0.196

Table 2. Servo characteristics [38].

Resolution	0.35°
Operating Angle Turn	300°, Endless
Voltage	7V~10V (Recommended voltage: 9.6V)
Max. Current	900mA
Operate Temperature	-5 °C ~ +85 °C
Command Signal	Digital Packet
Protocol Type	Half duplex Asynchronous Serial Communication (8bit, 1stop, No Parity)
Link (Physical)	TTL Level Multi Drop (daisy chain type Connector)
ID	254 ID (0~253)
Communication Speed	7343bps ~ 1 Mbps
Feedback	Position, Temperature, Load, Input Voltage, etc.
Material	Engineering Plastic



Figure 7. Front and back of actuators [38].

1.4. Movement of the robot. Gaits

Fundamental to the locomotion of animals is that they move by lifting their legs and placing them at new positions. While walking, the legs should be coordinated with respect to stability, propulsion and energy efficiency. The coordinated manner of lifting and placing the legs is called a gait. A gait is characterized by the sequence in which the legs are lifted and placed. The lifting or placing of a leg is called an event of the gait, and the sequence in which the legs are lifted and placed is called a gait event sequence. For a mobile robot with k legs, the total number of possible events N for a walking machine is $N = (2k - 1)!$ = **39916800** for a hexapod robot, but only a very small portion of them are suitable as gaits and used by animals [26]. Most people are familiar with the names of some of these gaits, for instance, a horse will switch between different gaits when increasing speed, first walk, then trot, then canter, and finally gallop. Animals switch gaits depending on speed in order to be more energy efficient, and the speed at which animals switch gait is dependent on the size of the animal. It has been noted that animals of different species use similar gaits for certain types of motion. A possible conclusion is that under some conditions of motion, a certain gait is optimum, for reasons that are related to stability, speed, energy efficiency, terrain properties, mobility or structure of the animal [27].

A gait is usually cyclic in the sense that the same sequence of lifting and placing the legs is repeated. A complete cycle of leg movements, where all the legs have been lifted and placed exactly once, is called a stride, and the time duration of one stride is called the cycle time. McGhee and Frank (1968) proposed a system, which is widely used today, where gaits are described in terms of duty factor and relative phase. The duty factor β_i for leg i is the fraction of the cycle time for which the foot is in ground contact, so the duty factor is a number between 0 and 1. The relative phase of leg i is the time elapsed from the setting down of an arbitrarily chosen reference foot until the foot of leg i is set down, given as the fraction of the cycle time. Thus the reference foot will be assigned the number 1, and has the relative phase $\varphi_i = 0$. The relative phases of the other legs are then:

$$\varphi_i = \frac{\Delta t_i}{T}, 0 \leq \varphi_i \leq 1, \quad (3)$$

Where Δt_i is the time elapsed since the reference foot was set down, and T is the cycle time. The gait event sequence can now be specified using the duty factors and the relative phases, where the first event, and the start of the stride, is chosen as the event when the reference leg is set down. The time, at which the following events of the gait will occur, are given as fractions of the cycle time at which the feet are set down or lifted. The timing of the events when the feet are set down is consequently equal to the relative phase φ_i . The timing of the events when the feet are lifted will be denoted ψ_i , and happens a fraction β_i of the cycle time after that the foot is set down. Alternatively, a foot has been lifted a fraction $1-\beta_i$ of the cycle time before it is set down again. However, as the events should be expressed within the duration of the stride, the events should be a number between 0 and 1. The event of lifting the leg i is given by:

$$\psi_i = \begin{cases} \varphi_i + \beta_i, & \text{if } \varphi_i + \beta_i < 1 \\ \varphi_i + \beta_i - 1, & \text{else} \end{cases} \quad (4)$$

For example, if the relative phase and the duty factor are $\varphi_i = 0.5$ and $\beta_i = 0.8$, respectively, then the event when leg i is lifted is $\psi_i = 0.3$. A gait is called singular if there is a simultaneous lifting or placing of two or more legs during the stride. A singular gait would correspond to that $\varphi_i = \varphi_j$, $\varphi_i = \psi_j$, or $\psi_i = \psi_j$, for any legs i and j where $i \neq j$. Any singular gait can be obtained as a limit of a non-singular gait [16].

Many walking algorithms have been developed for hexapod robots with limbs arranged symmetrically on either side of a longitudinal body axis, similar to an insect. Gaits for bodies with limbs arranged axially symmetric, have been defined by Song and Waldron [27], as:

Periodic

- **Wave gait:** stepping motions run from the rear to the front and legs on opposite sides of the body are 180 degrees out of phase
- **Equal phase gait:** all leg movements are ordered so that power consumption is consistent, like the wave gait motions run from rear to front
- **Backward wave gait:** similar to the wave gait except that motions run from front to rear
- **Backward equal phase gait:** similar to the equal phase gait except that motions run from front to rear
- **Dexterous periodic gait:** a follow the leader gait with the ability to adjust the placement of the two front feet
- **Continuous follow-the-leader gait:** feet are placed in the foot print of the foot ahead

Non-Periodic

- **Discontinuous follow-the-leader gait:** feet are placed in the foot print of the foot ahead, only one foot at a time is moved for greater stability

- **Large obstacle gait:** leg and body motions coordinate to traverse large obstacles while maintaining stability
- **Precision footing gait:** the operator either controls an individual leg with 3 DOF or controls the body with 6 DOF
- **Free gait:** used for avoidance of areas not suitable for weight bearing

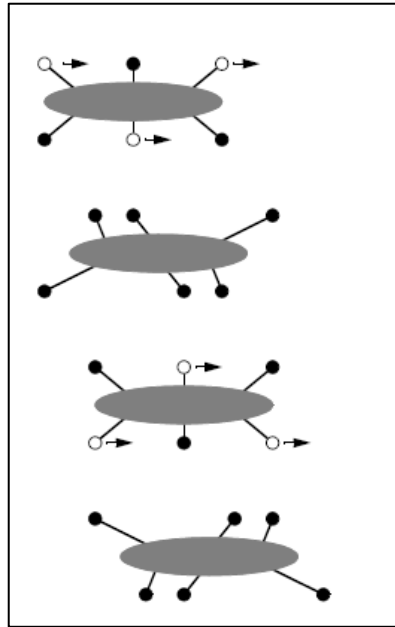


Figure 7. Detail of the tripod gait [39].

Periodic gaits are generally preferable because they are easily implemented and can provide smoother motion.

Various periodic wave gaits have been used for hexapedal robots, combined with biologically inspired coordination mechanisms found in stick insects [28].

While many walking algorithms [5, 10] would be suitable for such planar hexapedal locomotion, developing one sufficiently general enough to handle all navigable terrain and to utilize the kinematic structure of the robot adds complexity to the problem. The adaptable gait-planning algorithms under development are basic in the sense that they are currently only capable of planar locomotion, but general in that they could be used as the foundations for a more sophisticated algorithm capable of navigating complex terrain such as the surface of a spacecraft. It is also desirable that the basic elements of a walking algorithm be applicable in using the limbs to manipulate tools.

For these reasons, suitable base walking algorithms, while currently only capable of planar locomotion, must be capable of precise, pre-determined limb tip positioning. Also, the kinematic structure of the robot allows for body translation in any 3-space direction, as well as for pitch, yaw, and roll, while walking. Therefore, in order not to exclude mechanical capabilities, the base algorithm

will be capable of instantaneously and simultaneously executing any combination of translations and change of orientation of the body while walking.

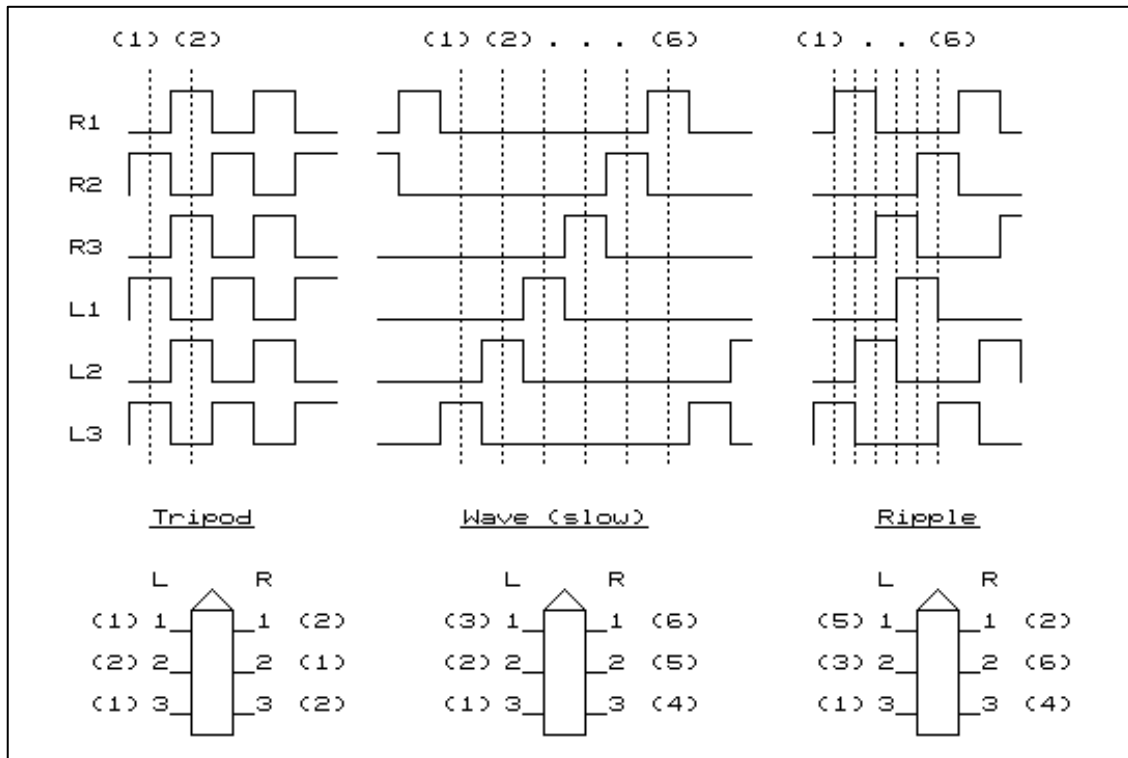


Figure 8. On/off states of the servos during a stride in different types of gaits [40].

1.5. What is stability?

In order to put walking vehicles into practical use for the above application, they must manage to keep walking slowly but as stably as possible, even if they traverse rough terrain including slopes. From this point of view, it is indispensable to define the most reasonable stability criterion for walking vehicles and to design a gait maximizing its margin. Needless to say, several stability criteria have been proposed up to now. They can be divided in two groups, static and dynamic stability margins, but as we will see later, the dynamic effect is added to the each static stability margin [31].

1) “**Stability Margin**”: It evaluates the distance between the projection of the center of gravity on the ground and the border of the polygon formed by the supporting feet of the walking vehicle on the plane.

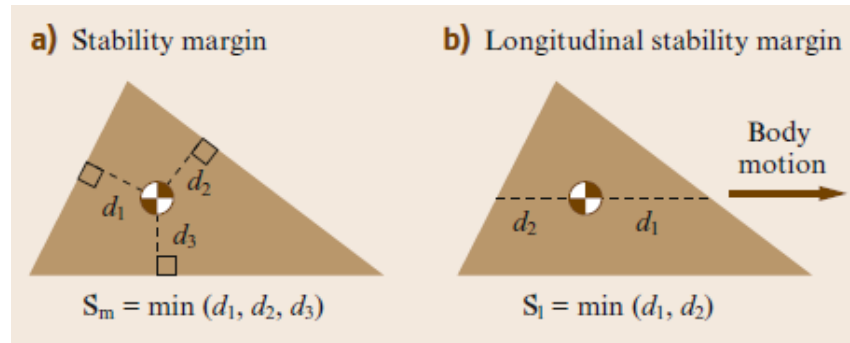


Figure 9. a) Static stability margin, b) longitudinal stability margin [41].

2) “**Tumble Stability Margin**”: When the walking vehicle tumbles around the line connecting two support feet, it evaluates the absolute value of the moment divided by its weight which generates around the line to avoid tumbling. It corresponds to the “Stability Margin” ignoring the dynamic effect when the walking vehicle is on the level ground.

3) “**Gradient Stability Margin**”: It evaluates the inclination of the walking vehicle at which it starts tumbling owing to gravity, when it gets inclined little by little from the level ground.

4) “**Tipover Stability Margin**”: It is similar to the criterion of the “Gradient Stability Margin,” but all the external forces including gravity are considered to work on the center of gravity of the walking vehicle.

5) “**Energy Stability Margin**”: In the process of tumbling, the center of gravity passes over the point at which it possesses the maximum potential energy under the field of gravity. This criterion evaluates the stability by the magnitude of the difference between its maximum potential energy and its initial one.

6) “**Dynamic Energy Stability Margin**”: It is similar to the criterion of the “Energy Stability Margin,” but all the external forces including gravity are considered to work on the center of gravity of the walking vehicle.

The criteria of 2), 4), and 6) add the dynamic effect to the criteria of 1), 3), and 5) respectively. The best way to evaluate the behavior and results of each stability criteria is to put the robot under hard conditions of the terrain, for example a sloped ground. In the next figures we will see how the different stability margins determine different positions of the CG in order to improve stability.

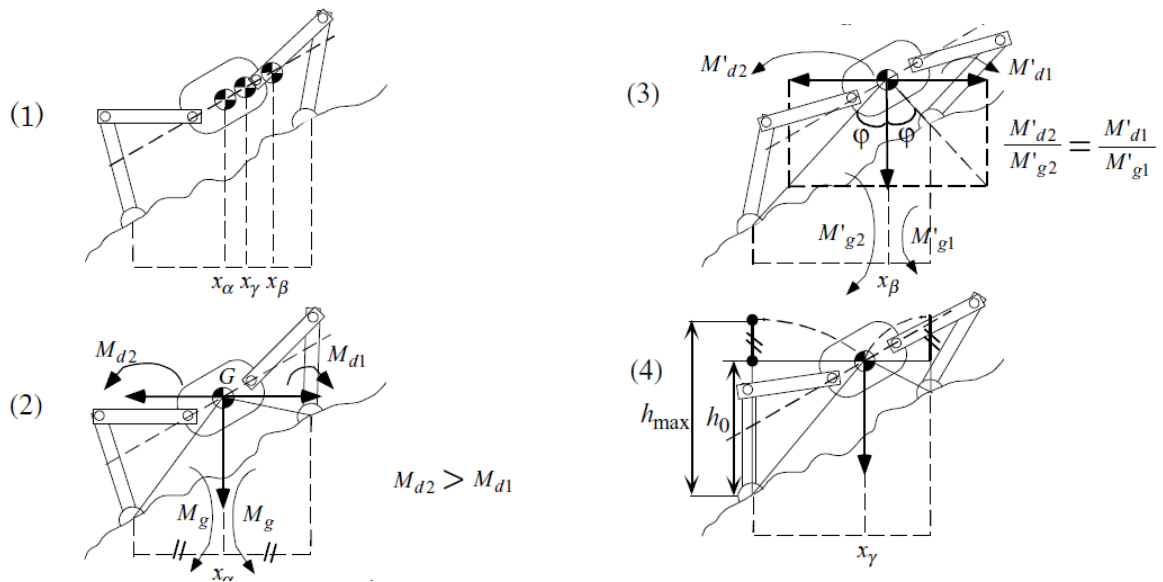


Figure 10. The relationship between the posture and stability criterion. (1) The walking vehicle under consideration. (2) Posture maximizing the Stability Margin. (3) Posture maximizing the Gradient Stability Margin. (4) Posture maximizing the Energy Stability Margin [31].

The criterion 1) was proposed on the assumption that walking vehicles were on the level ground, but it is contradictory on the rugged slope shown in Fig. 11(1), where the walking vehicle touches the ground by its two feet in 2D. Then let's consider the most stable point for the center of gravity on the line at the constant height from the ground. According to the "Stability Margin," the most stable posture is the one shown in Fig. 11(2), where the center of gravity is situated just in the middle. It is true that this posture can maximize the minimum moment (M_g) by gravity around each foot which works to stabilize the body. However, once the body is affected by a disturbance force from the horizontal direction, the moment around the downhill foot (M_{d2}) becomes larger than that around the uphill one (M_{d1}) and it is easier for the walking vehicle to tumble down the slope, even if the sizes of the disturbance force are kept equal. Consequently, the "Stability Margin" doesn't give us a right result, when all the support feet are not on the same level plane. Considering the fact that the moments (M'_{d1} , M'_{d2}) caused by the horizontal disturbance forces differ in each support foot, the posture should be changed so that M'_{d1} , and M'_{d2} generates in proportion to M'_{g1} and M'_{g2} respectively. Such a posture is expressed by Fig. 11(3) at which the resultant vector of both gravity and the horizontal force vectors pass over each support foot. As a result, it corresponds to the posture maximizing the "Gradient Stability Margin," which evaluates the inclination of the waling vehicle on rough terrain when it starts tumbling by the instant disturbance force. From these points of view, another consideration comes up to our mind, which regards the cause of the tumble as not the instant force but as the energy working on the body. More specifically, the center of gravity won't reach its highest position in the process of its rotating around the support foot, if its kinematic energy by the disturbance is completely consumed by increasing its potential energy. In other words, a large difference between the potential energy at the

initial position of the center of gravity and one at its highest position can evaluate the stability of walking vehicles from the energy point of view. This difference was proposed as the “Energy Stability Margin.”

This criterion shows us that the posture in Fig. 11(2) is easier to tumble down the slope because the lifted distance of the center of gravity for the downhill side is less than that for the uphill side, while the posture in Fig. 11(3) is easier to tumble to the uphill side. As a result, the most stable posture maximizing the Energy Stability Margin is one in Fig. 11(4) which divides it equally into both sides. Eventually, these criteria lead to a different optimal position of the center of gravity respectively, as shown in Fig. 11(1), but which one is the most reasonable for the practical use?

1.5.1. Energy stability margin, ESM

Several authors conclude that it is better to evaluate the stability by means of the “Energy Stability Margin”. However, some inconvenient aspects remained in this criterion when it is used without any modification. According to the definition of “Energy Stability Margin”, walking vehicles would become more stable in proportion to its weight, even though their posture doesn't change at all. But at the same time, the disturbance acting on the center of gravity also becomes large with the increase of weight; therefore, the increase of weight does not necessarily leads to the increase of stability. On account of this reason, the static stability criterion should be expressed by the dimension of length without including weight, that is, it should be defined as just the vertical distance between the initial position of the center of gravity and its highest position in the process of tumbling. Also ESM still does not consider any dynamic effects that might disturb vehicle stability.

1.5.2. Normalized Energy Stability Margin, NESM

“Normalized Energy Stability Margin” or “NE Stability Margin” for short, as expressed in the following equation:

$$S_{NESM} = \frac{S_{ESM}}{mg} = \min_i^{np}(h_i) \quad (5)$$

Although “NE Stability Margin” doesn't change essentially from “Energy Stability Margin”, it has a few advantages as follows.

- i) Stability can be evaluated in proper way when such a disturbance as mentioned before occurs.
- ii) As it is expressed by not the unit of [J] but the unit of [mm], it is convenient to derive a gain by means of the geometric way.

iii) When walking vehicles are on the ground, “NE Stability Margin” corresponds to “Stability Margin” in the case where the center of gravity touches to the ground, which has the continuous relationship and is easier to understand intuitively.

However, when dynamic effects arise during walking, machine stability cannot be judged precisely. Such situations exist in real walking robot applications, and therefore dynamic stability margins are more suitable.

1.5.3. Dynamic stability margin, DSM

To solve the unusefulness of static stability margins when robot dynamics are relevant some momentum-based stability criteria have been defined. Lin and Song [17] defined the Dynamic Stability Margin, DSM, as the smallest of all moments M_i around the edges of the support polygon caused by robot/ground interaction forces, normalized by the weight of the system, that is:

$$S_{DSM} = \min_i \left(\frac{M_i}{mg} \right) = \min_i \left(\frac{e_i \cdot (F_R \times P_i + M_R)}{mg} \right) \quad (6)$$

Where P_i is the position vector from the CG to the i -th support foot, F_R and M_R are the resultant force and moment of robot/ground interaction, and e_i is a unit vector that revolves around the support polygon in the clockwise sense. If all moments are positive (if they have the same direction and sense as e_i), then the system is stable.

1.5.4. Force-Angle Stability Margin, FASM

A different criterion was proposed by Papadopoulos and Rey 18. The Force-Angle stability criterion finds the angle α_i between the resultant force acting from the CG on the ground (the opposite to the reaction force F_R) and the vector R_i , normal to the rotation axis from the CG. The system becomes unstable when this angle becomes zero. The stability margin is the product of the angle times the resultant force F_R , that is:

$$S_{FAASM} = \min(\alpha_i) \cdot \|F_R\| \quad (7)$$

These are the main stability criteria used for comparison with the herein proposed one. Recent research has demonstrated that none of the static stability margins are suitable for measuring robot stability when robot dynamics are relevant. The FASM seems to be the best of the existing margins, because it accurately judges stability on flat terrain in the presence of inertial effects. However, it loses accuracy when manipulation effects arise or when the robot walks over uneven terrain.

Furthermore, it shows that none of the dynamic stability margins accurately measure stability when there are manipulation forces and moments or dynamic effects during the transfer of the legs.

1.5.5. Normalized Dynamic Stability Margin, NDSM

The optimum stability margin from the energy viewpoint is the one that quantifies the maximum impact energy that the machine can absorb without losing stability. Following this definition, the ESM is optimum under static conditions, e.g. when the only significant force acting on the robot is gravity. The ESM is computed from the increase of potential energy that the machine's *CG* experiences when pivoting around the edges of the support polygon. Therefore, the extension of the ESM to the presence of other robot dynamics, like inertial forces or manipulation effects, must compute the increase of mechanical energy that the *CG* experiences during the tumble. This idea was proposed by Ghasempoor and Sepehri 24 to measure robot stability in the application to wheel-based mobile manipulators. In this paper, Ghasempoor and Sepehri's idea has been extended to walking machines, considering leg dynamics as a destabilizing effect.

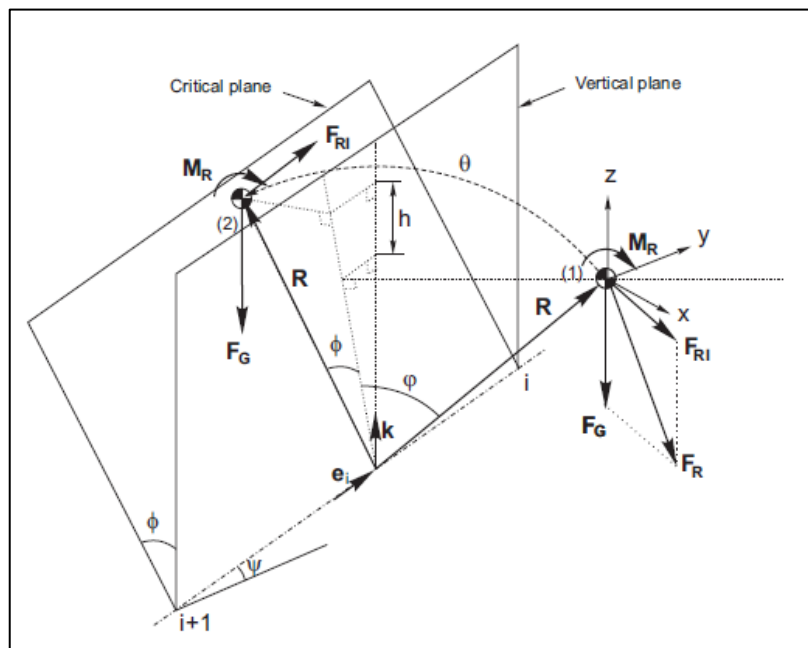


Figure 11. Geometric outline for the computation of the NDESME [31].

Let us consider a walking robot during its motion, where gravitational, inertial and manipulation forces and moments become significant. At a given instant an external impact causes the robot to tumble around one edge of its support polygon. The impact is caused by a force that interacts with the robot during an infinitesimal interval of time. Therefore, any joint motion during this interval is negligible and thus the robot will be considered as a rigid body.

Figure 12 depicts the *CG* of a robot during the tumble around the edge of its support polygon, given by the line connecting footprints i and $i + 1$. This edge is inclined at an angle θ from the horizontal plane due to terrain inclination. If the moment around this rotational axis caused by the resultant forces and moments of robot/ground interaction, F_R and M_R , is able to compensate for the destabilizing effect, the robot could maintain stability. If, on the contrary, the effect cannot be compensated for, the robot will lose stability. Therefore, the instant of critical stability occurs when the moment of robot/ground interaction forces and moments around the rotation axis vanishes. At that time the *CG* is located inside a critical plane that forms an angle ϕ with the vertical plane (see position (2) in Figure 12).

At the initial position (1) before the tumble, the *CG* is subject to inertial forces and moments (F_I and M_I), gravitational forces and moments (F_G and M_G), and manipulation forces and moments (F_M and M_M). The perturbing effects of a leg in transfer phase can be also considered as manipulation terms. Assuming that the dynamics of the legs in the support phase is negligible relative to the body dynamics, the resultant force and moment of robot/ground interaction are given by:

$$\begin{aligned} F_R &= F_G + F_M - F_I \\ M_R &= M_G + M_M - M_I \end{aligned} \quad (8)$$

During the tumble from position (1) to position (2), the gravitational force, F_G , remains constant, while the rest of forces and moments rotate with the robot reference frame. Therefore let us divide the resultant robot/ground interaction forces, F_R , into two components: one gravitational and the other non-gravitational. Let us name the non-gravitational component F_{RI} , that is:

$$F_{RI} = F_R - F_G \quad (9)$$

The mechanical energy increase experienced by the *CG* during the tumble from position (1) to position (2) is given by the following energy balance:

$$E_i = V_2 - V_1 + K_2 - K_1 \quad (10)$$

Where V_1 and K_1 are the potential and kinetic energies of the *CG* respectively before the tumble (1), and V_2 and K_2 are the potential and kinetic energy of the *CG* at the critical plane. Inside the critical plane the resultant moment around the rotation axis vanishes, thus the rotational speed of the *CG* is zero at this time, therefore:

$$E_i = V_2 - V_1 - K_1 \quad (11)$$

The increase of potential energy, $V_2 - V_1$, is the sum of potential energy due to gravity, F_G , and the rest of forces and moments, F_{RI} and M_R , that is:



$$V_2 - V_1 = \Delta V_G + \Delta V_F + \Delta V_M \quad (11)$$

$$\Delta V_G = mgh \quad (14)$$

$$\Delta V_F = \int_{\theta_1}^{\theta_2} (F_{RI} \times R) e_i d\theta \quad (15)$$

$$\Delta V_M = \int_{\theta_1}^{\theta_2} (M_R \cdot e_i) d\theta \quad (16)$$

To compute the kinetic energy of the system before the tumble the following equation must be solved:

$$K_1 = \frac{1}{2} I_i w_i^2 \quad (17)$$

Where I_i is the moment of inertia around the rotation axis, which is known, and w_i is the angular speed of the robot before the tumble, which is obtained from:

$$w_i = \frac{L_i}{I_i} \quad (18)$$

Let us consider the speed of the CG before the tumble (1) v_{CG} . Then, the angular momentum L_i is computed from:

$$L_i = (R \times m v_{CG}) \cdot e_i \quad (19)$$

Where m is the total mass of the robot and its manipulator system. Then the kinetic energy of the system before the tumble can be obtained by substituting equations (18) and (19) in (17). Thus the term E_i in equation (10) is the increase of mechanical energy of the CG when pivoting around the edge i of the support polygon. It is also the increase of the machine's stability level when the machine is rotating around that axis due to an impulsive perturbation. Therefore let us propose the following definition:

We would say that a walking machine is dynamically stable if every moment M_i around the i -edge of the support polygon due to robot/ground forces and moments is positive, with the vector that goes around the support polygon in the clockwise direction being positive, that is:

$$M_i > 0, i = 1..n - 1 \quad (20)$$

Where i is the edge of the support polygon, and n is the number of supporting feet. M_i is the moment around the axis i and comes from:

$$M_i = ((F_{RI} + F_G) \times R + M_R) \cdot e_i \quad (21)$$

If equation (20) is true the robot is stable, and then the Normalized Dynamic Energy Stability Margin is defined as:

Normalized Dynamic Energy Stability Margin is the smallest of the stability levels required to tumble the robot around the support polygon, normalized to the robot mass, that is:

$$S_{MEEDN} = \frac{\min(E_i)}{mg} \quad (22)$$

Where E_i is the stability level, given by (10).

For the validation of this method, a simulation and a quadruped robot were used in [31]. The results show that for static conditions, the NDESM and the NESM coincide, proved both to be optimum. Moreover, while NDESM is subject to inertial and manipulation effects, NDESM is able to predict robot stability precisely for different ground profiles and different dynamic effects perturbing motion, including robot inertia and manipulation dynamics.

1.6. Analysis of relationship between stability margin and dexterity

In the process of design, the structure parameters are optimized to improve the dexterity at utmost [33]. However, when robot is walking, the support positions of stance legs and the gait pattern have great influence on dexterity as well as the stability margin. It is desired that the robot has a better dexterity while satisfying the utmost stability margin. The analysis is as follows. As shown in Fig. 13, robot is assumed to stand on a flat terrain, the vertical projection of CG is taken as the origin of the reference, X, Y, Z are coordinate axis, the locations of each stance foot are shown as the points P_1 to P_6 . The stability margin R_{sm} is defined as the shortest perpendicular distance from the vertical projection of CG to each side of SP. The value of stability margin is relevant to the position of CG relative to the support points of the stance-legs. The dexterity is indicated by the workspace of the trunk. The workspaces of trunk for different number of stance legs and different support positions of stance-legs are calculated using MATLAB.

Fig. 13(a) is the comparison of dexterity of trunk with three stance-legs and six stance-legs while the homologous legs have the same support positions. It can be inferred that dexterity decreases with the increase in the number of stance legs, and the stability margin increases.

Fig. 13(b) is the comparison of dexterity of trunk with different support positions of homologous legs for the same number of stance legs. It can be deduced that the dexterity increases with the decrease in the support polygon, and the stability margin decreases simultaneously. Through above

analysis, it is realized that the stability margin and dexterity of the hexapod robot are a couple of incompatible factors that fail to reach their optimal values at the same time. Accordingly, when the robot is at rest, more care to the dexterity should be taken to prepare the following movement. When the robot is walking on unstructured terrain, the posture control must be employed for improving the stability margin on-line [45].

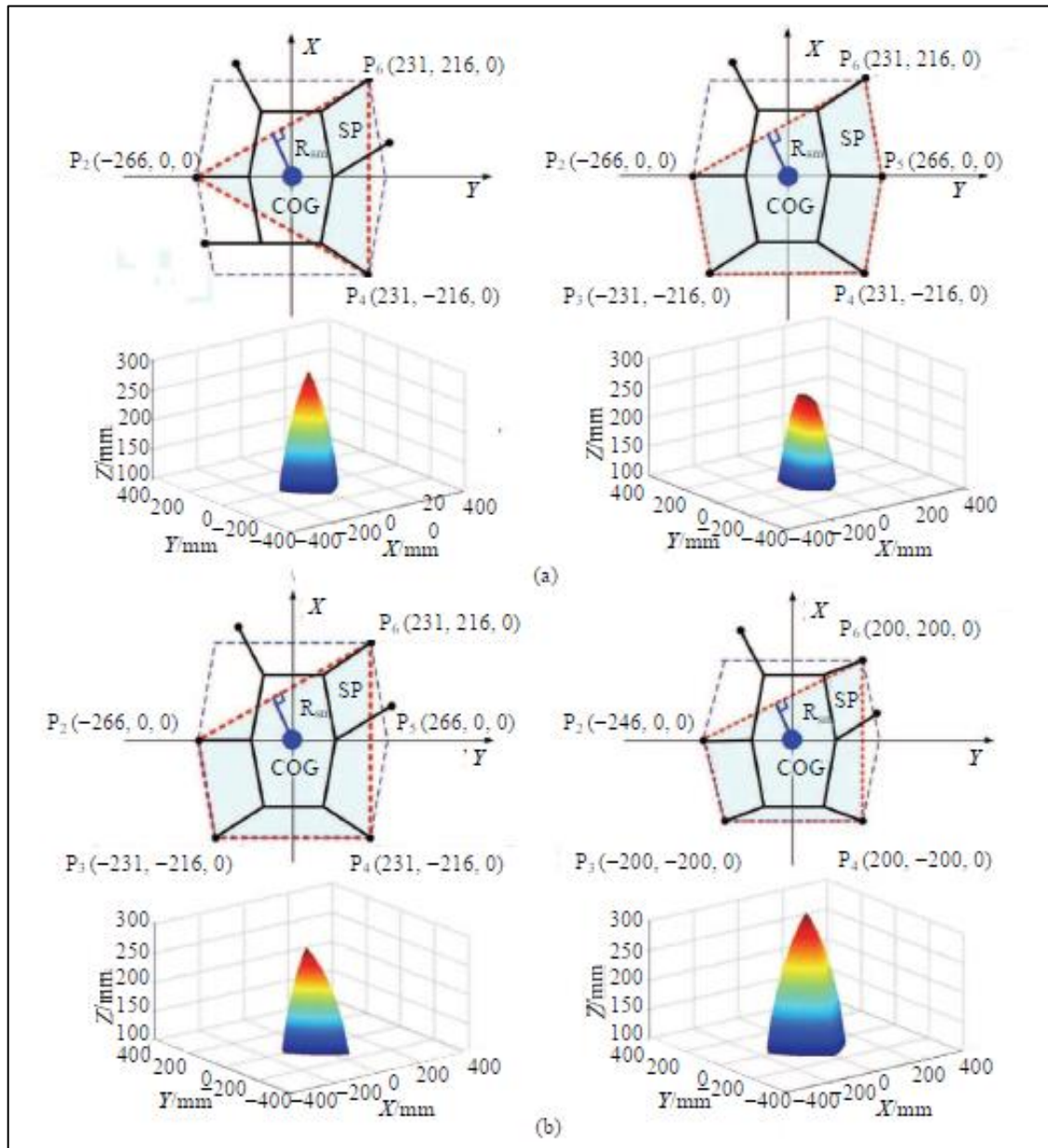


Figure 12 Comparison of dexterity of trunk: (a) different number of stance-legs while homologous support points are same; (b) different support points while the number of stance-legs is same [45].



1.7. Terminology

The definitions are in alphabetical order, and based on Alexander (1984), Kumar, and Waldron (1989), Song, and Waldron (1989), and Wadden (1998) [16].

- **Duty factor (β):** The fraction of the duration of the stride for which a foot is on the ground (in the support phase). Duty factor can be used to make the distinction between walks and runs, since we have $\beta \geq 0.5$ for walking and $\beta < 0.5$ for running.

$$\beta = \frac{\text{support period}}{\text{cycle time}} \quad (23)$$

- **Cycle time (T):** Time duration of one stride, i.e. the time to complete one cycle of leg movements.
- **Events of the gait:** The placing or lifting of any of the feet during locomotion. For an n-legged machine, there are 2n events in one stride.
- **Relative phase (φ_i):** The time elapsed from the setting down of a chosen reference foot until the foot of leg i is set down, given as the fraction of the cycle time.
- **Stability margin:** The shortest distance from the vertical projection of the center of gravity of the robot onto a horizontal plane, to the boundary of the support area.
- **Stride:** The complete cycle of leg movements, for example, from the setting down of a particular foot to the next setting down of the same foot, where all the legs have been lifted and placed exactly once.
- **Stride length:** The distance travelled by the center of gravity of the walker in one stride.
- **Leg Stroke (R_x):** The distance that foot i translates relative to the hip during the support phase.
- **Stroke pitch (P_x):** Is the distance between the centers of the workspaces of adjacent legs on one side. Depends on the geometry of the walking robot.
- **Support area/polygon:** The minimum convex polygon in a horizontal plane, with its vertices formed by the vertical projection of the feet being in support.
- **Support phase:** The phase when a foot is in contact with the ground and able to support and propel the body. Also called stance or retraction phase.
- **Swing phase:** The phase when a foot is in the air and repositioned for the next support phase. Also called air or protraction phase.

2. DEVELOPMENT OF THE ROBOT

2.1. Design Considerations

Designing hexapod legged robots is far from trivial. A very numerous and a wide range of possibilities exist to design a hexapod as also described in the previous section. Designers must take several decisions which influence the operation and technical features. Some of the most important design issues and constraints according to [25] can be outlined as:

- The mechanical structure of robot body;
- Leg architecture;
- Maximum sizes;
- Actuators and drive mechanisms;
- Control architecture;
- Power supply;
- Walking gaits and speed;
- Obstacle avoidance capability;
- Payload;
- Autonomy;
- Operation features;
- Cost.

The above mentioned design issues and constraints can be classified as design input (or key features) and design output (or main design characteristics) as shown in the scheme of Fig. 14.

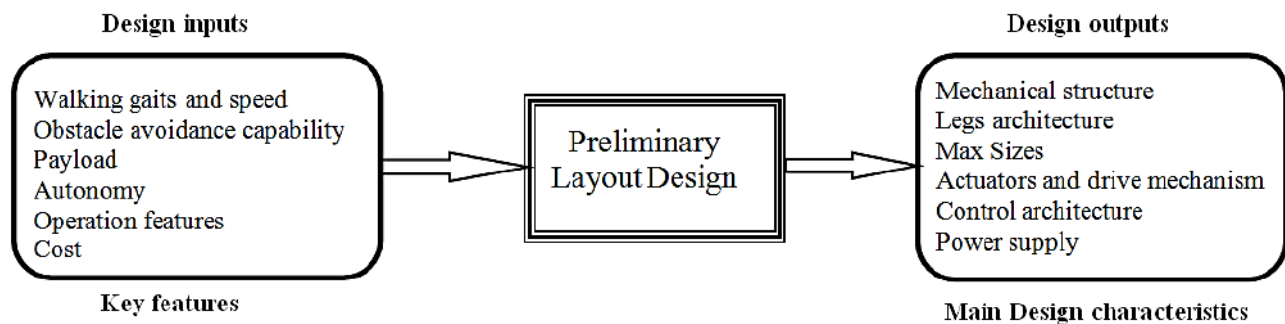


Figure 13. A scheme for preliminary layout design of hexapod walking robots [9].

A survey on the state of the art shows that each hexapod walking robot design is almost unique. Hexapod can be developed in several configurations and every solution has its design criteria, specifications, shapes, advantages and disadvantages, but the literature is lacking a systematic design procedure for hexapod robots as referring to specific functional requirements.

2.2. Modeling

The development of the body for the new hexapod robot starts from defining some parameters that will determine other variables of the robot, such as, for example, the size of the legs is crucial for the step length. Some of them can be easily changed, because they have not been built yet. On the other hand, the structure of the leg for example, cannot be modified, as we will use the ones already constructed from the old prototype.

2.2.1. Leg structure

First, the properties of the legs. Each of the six legs will have three servos AX-12, which will provide three degrees of freedom.

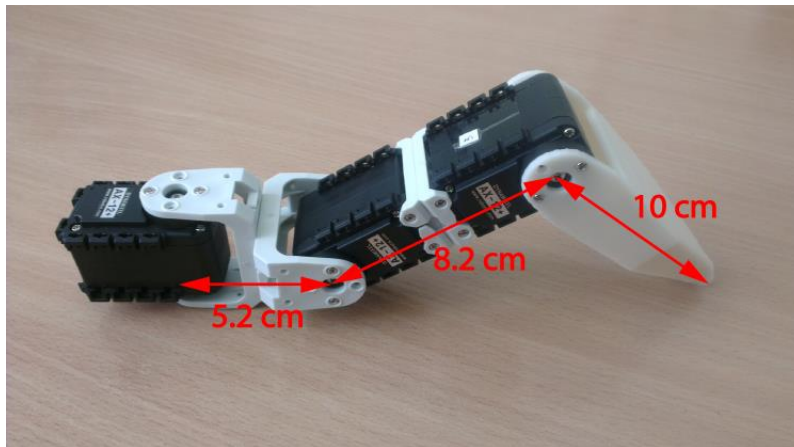


Figure 14. Real leg of the hexapod

For the static position of the legs, we will select 0° of femur articulation, 0° of tibia articulation and 90° of tarsus articulation, which has a projection on the plane XY of $L=13.4$ cm. This is a first approach, because the projection of the leg is needed to optimize the body configuration. Later when the step length is discussed, the configuration of the leg may change. Moreover, a step length of 5cm is set as default (30° of femur articulation).

2.2.2. Design of the body

Based on the premise that the body is thought to be rectangular, we should decide its dimensions. It should be considered the size of the body to be the smallest as possible, because we will reduce the weight of the whole prototype. However, there are parts of the robot, as the microprocessor, the batteries or the sensors that will be placed over the body. Those parts will determine the size. With the

information provided in the datasheet of the microprocessor and the servos as well as the feedback from the old prototype, we set an initial dimension for the body:

$$\text{Large}=25 \text{ cm}; \quad \text{Width}=15 \text{ cm}$$

We check that placing the microprocessor in the center of the body, everything fits inside. We will place the leg so that the axis of the femur articulation matches with the boundaries of the body:

- Part of the leg inside the body=38.5 mm (owning to the femur servo)
- Width of microprocessor board=70 mm

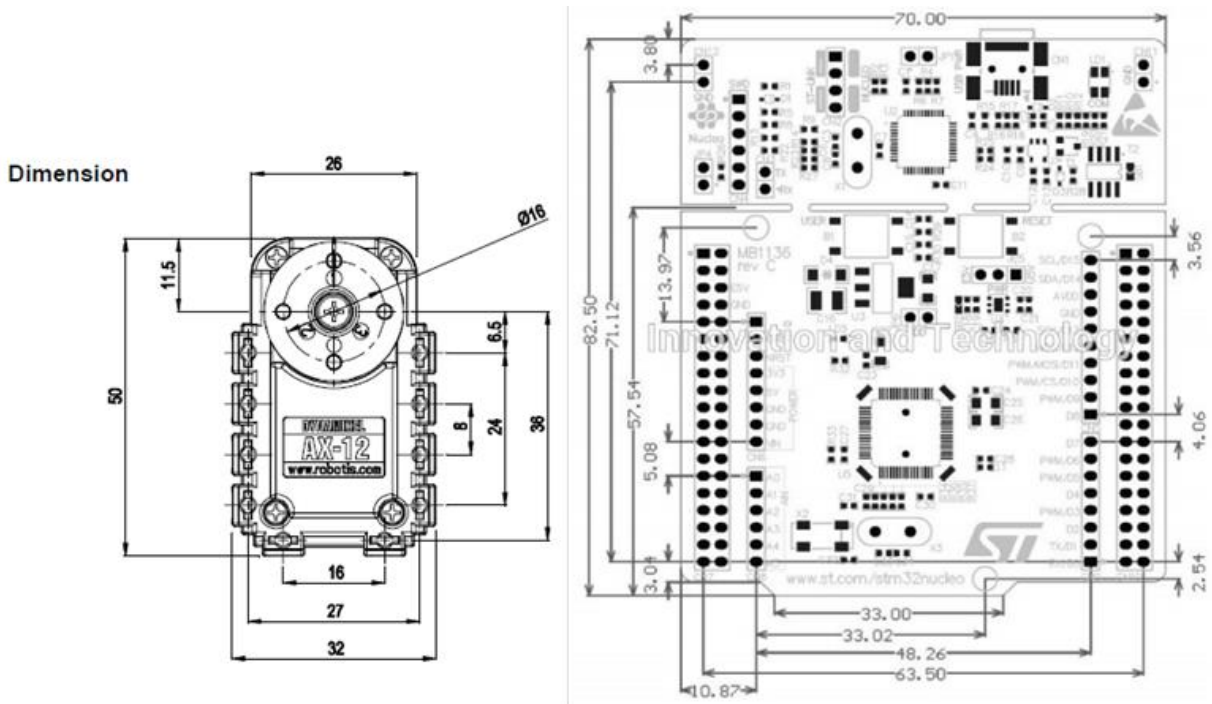


Figure 15. Dimensions of the servo and the microprocessor [38]

$$38,5 \cdot 2 + 70 = 147 < 150\text{mm}$$

The microprocessor and sensors will be placed over the body in the center of it. This will provide equilibrium and will keep the center of gravity as centered as possible. It will become a rule in the design, because the symmetric bodies possess the highest stability. The front and rear legs will be placed in the corners, while the middle legs will be place at equal distance from the corner legs of each side. Every leg will lay attached to the body, trying to match the coxa axis with the boundaries of the body.

2.2.3. Displacement of the middle legs

Walking robots are intrinsically slow machines, and machine speed is well known to depend theoretically on the number of legs the machine has [34]. Although stability is no optimum when using alternating tripods, tripod gait is the most widely used by hexapods. “Alternating tripods” means those two non-adjacent legs on one side and the middle leg on the opposite side alternate in supporting the robot.

To analyze the leg forces that a hexapod must exert, we will consider an insect leg configuration as in Fig. 17 where all leg workspaces lie in the same relative position with respect to the longitudinal axis of the body. The equilibrium equations that balance forces and moments, in the support phase are given by:

$$A * F = W$$

$$A = \begin{pmatrix} x_2 & x_3 & x_6 \\ y_2 & y_3 & y_6 \\ 1 & 1 & 1 \end{pmatrix} \quad (24)$$

$$F = (F_2, F_3, F_6)^T$$

$$W = (0, 0, -W)^T$$

Where F_i is the vertical ground-reaction force in foot i , $((x_i, y_i))$ are the position components of foot i in the robot’s reference frame (X, Y, Z) and W is the robot’s weight.

The robot is assumed to describe a continuous alternating tripod gait that consists in two main phases. In the first phase, legs 1, 4 and 5 are in support and moving backwards at a constant speed (continuous gait), while legs 2, 3 and 6 are in support. Each supporting leg follows a straight-line trajectory on the ground parallel to the trajectory of the other supporting legs.

It will be consider as “leg stroke”, R_x , the distance through which the foot is translated relative to the body during the support phase. The “stroke pitch”, P_x , is the distance between the centers of the workspaces of the adjacent legs on one side. The body length L_B , the distance from the foot trajectory to the origin of the leg reference frame L , and the distance between the leg reference frames of non-collateral adjacent legs, D .

The components of the position of the foot at any time will be:

$$(x_i(k), y_i(k), z_i(k)) = G(k, i); \quad \text{for } i = 1, \dots, 6 \quad (25)$$

$$x_i(k) = \sigma(i)P_x + (-1)^{\xi \left(\frac{k}{N+1} \right)} R_x \left(\frac{1}{2} - \frac{1}{N-1} \left(((k-1) \bmod N) - 1 \right) \right); \quad (26)$$

for $i = 1, \dots, 6; k = 1, \dots, 2N$

$$y_i(k) = (-1)^{i+1} \left(\frac{D}{2} + L \right); \tag{27}$$

for $i = 1, \dots, 6; k = 1, \dots, 2N$

$$z_i(k) = \begin{cases} h \sin\left(\frac{\pi k}{N}\right) \left(1 - \xi\left(\frac{k}{N+1}\right) \right) - H & \text{for } i = 1, 4, 5; k = 1, \dots, 2N \\ -h \sin\left(\frac{\pi k}{N}\right) \left(\xi\left(\frac{k}{N+1}\right) \right) - H & \text{for } i = 2, 3, 6; k = 1, \dots, 2N \end{cases} \tag{28}$$

Where k is the sample period, i is the leg number and G is the gait vector function defined by:

Where $2N$ is the number of samples in a locomotion cycle, H is the height of the body and h is the step height over the ground. Function $\sigma(i)$ defines the displacement of the body attachment of leg i with respect to the center of the body reference frame (X , Y , and Z) and is given by:

$$\sigma(i) \begin{cases} 1; & \text{for a front leg} \\ 0; & \text{for a middle leg} \\ -1; & \text{for a rear leg} \end{cases} \tag{29}$$

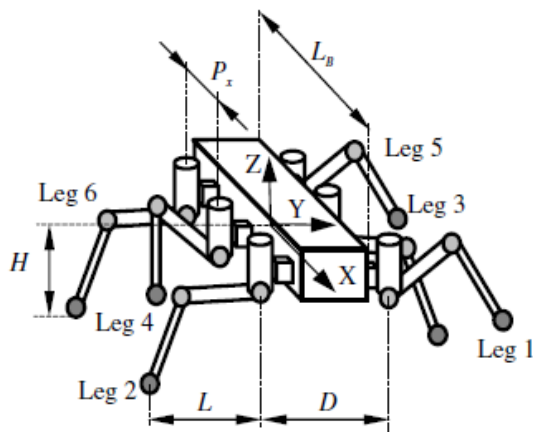


Figure 16. Geometric model of normal walking robot [34].

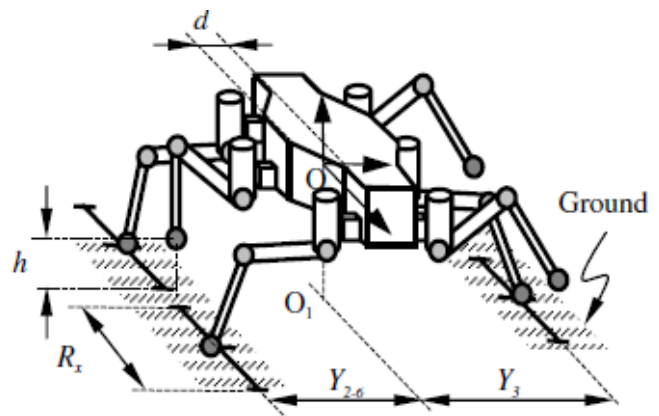


Figure 18. Geometric model of modified walking robot [34].

Function $\xi(x)$ is the function fix, which rounds the element x to the nearest integers towards zero and mod represents the function module.

It is needed to mention that the leg trajectory for the component z could be defined as a polynomial function, trigonometric function and so on. The sine function has been chosen, although it does not affect to the final result as we will see later.

With these foot positions, the foot forces along a whole locomotion cycle can be computed as:

$$F = A^{-1}W \quad (30)$$

Having an expression for the whole locomotion cycle:

$$\begin{aligned} \begin{pmatrix} F_1(k) \\ F_4(k) \\ F_5(k) \end{pmatrix} &= \left(1 - \xi \left(\frac{k}{N+1} \right) \right) \begin{pmatrix} x_1(k) & x_4(k) & x_5(k) \\ y_1(k) & y_4(k) & y_5(k) \\ 1 & 1 & 1 \end{pmatrix}^{-1} \begin{pmatrix} 0 \\ 0 \\ -W \end{pmatrix} \\ \begin{pmatrix} F_2(k) \\ F_3(k) \\ F_6(k) \end{pmatrix} &= \left(\xi \left(\frac{k}{N+1} \right) \right) \begin{pmatrix} x_2(k) & x_3(k) & x_6(k) \\ y_2(k) & y_3(k) & y_6(k) \\ 1 & 1 & 1 \end{pmatrix}^{-1} \begin{pmatrix} 0 \\ 0 \\ -W \end{pmatrix} \end{aligned} \quad (31)$$

for $k = 1, \dots, 2N$

When a legged robot is supported by a tripod, the middle leg in its support phase, for a given foot position, is carrying about half the robot's weight, while the two collateral legs in their support phase are carrying about one-fourth of the robot's weight.

Satisfactory force distribution and system homogenization can be achieved by shifting the middle legs' foot positions slightly from the body's longitudinal axis so that the middle legs support less weight and the corner legs increase their contribution to supporting the body. By displacing the middle leg attachment points the support polygon increases, therefore, the static stability margins also increases.

If we only considered the geometric distribution of the legs, we can reach an optimum point for the distance between the longitudinal axis and the new position of the middle leg that is the double of the distance between that longitudinal axis and the attachment point of one corner leg. Nevertheless this study should be performed along a whole locomotion cycle, and the central leg-attachment point should be moved such that the maximum foot force in any middle leg equals the maximum foot force in any lateral leg.

For that is necessary to recalculate the foot forces for every foot position along a locomotion cycle. Then the middle leg displacement can be calculated so that it will eliminate the difference between a middle leg maximum force and a lateral leg's maximum force.

From the equations described before, we will only modify the component x and y. The component x will be added a new parameter OffsetX, which will represent the displacement of the rear and front legs along x axis if we set a default offset for those legs. How this will affect to stability will be discussed later. The parameter d will be the displacement of a middle leg with respect to a lateral leg along the direction of the Y-axis.



$$x_i(k) = \sigma(i)P_x + OffsetX + (-1)^{\xi\left(\frac{k}{N+1}\right)}R_x\left(\frac{1}{2} - \frac{1}{N-1}\left(\left((k-1)\bmod N\right) - 1\right)\right);$$

for $i = 1, \dots, 6; k = 1, \dots, 2N$

$$y_i(k) = \begin{cases} (-1)^{i+1}\left(\frac{D}{2} + L\right) & \text{for } i = 1, 2, 5, 6 \\ (-1)^{i+1}\left(\frac{D}{2} + L + d\right) & \text{for } i = 3, 4 \end{cases} \quad (32)$$

Then the problem is reduced to finding the parameter d that yields:

$$\theta(d) = 0 \quad (33)$$

Where

$$\theta(d) = \max_k(F_1(k, d)) - \max_k(F_3(k, d)) \quad (34)$$

In other words, we move the point where the middle legs (3,4) are attached until the maximum foot force in the middle legs equals the maximum foot force in the lateral legs (1,2,5 and 6) [34].

2.2.4. Offset in the coxa angle in front and rear legs

Less investigation has been made in the offset for the coxa angle of corner legs. It is clear that the biggest offset angle in the corner legs the robot has, the more similar behavior to a circular body robot will have. This is a better turning ability, higher stability margin and greater stride length in certain conditions. However, the rectangular configuration has also its advantages, as we discussed in section 1.1. This angle also affects to the step length of the robot, as a greater distance between each leg from the same size will provide robot with a bigger step length, and therefore higher speed. So the simulation will have to look for an angle that will provide equilibrium between high speed, great step length and static stability margin.

2.2.5. Models

Now it is time to work on the model of the robot and try to improve it. First we will modify the offset of the coxa angle. Second, we will program a code in *Mathematica* to get the displacement of the middle legs in each configuration. This code will be based on the explanation given on section 2.2. Later a set of three different leg configuration are proposed. With this tree configuration we will get



each maximum step length. Once every parameter is analyzed, we will decide the final design and draw it using *Autodesk Inventor*. The final result will be shown below.

As we said, we will start by analyzing the robot's static stability by modifying the offset of the coxa angle. All the data will be displayed in the International Unit System (mm).

The first results are reflected in Table 3. From this table it is easy to observe that the bigger the offset angle is, the bigger the stability margin and longitudinal stability margin become. Nevertheless, for a big offset angle we will require a leg able to extend a bigger distance for the same step length. For example, with a steplength of 5cm and an offset angle of 30° , the extension required for the leg to place the foot in the next point (remember the foot always moves in a straight line for an straight walking) is $134+45.5=179.5\text{mm}$, while for an offset of 0° is $134+9=143\text{mm}$. This will reduce our possible options.

Now we will use the algorithm for optimizing the placement of the middle leg. The algorithm is included in Annex I. We will change the width of the body because if we move the middle legs, we have more space in the body for the microprocessor. Another thing to be considered is the static position of the corner legs. This algorithm is designed so that every leg of each side is placed in the same distance to the longitudinal axis of the body, so we will extend the corner legs in the configurations with angle offset so that we reach the straight line defined by the middle leg. Once calculated the distance to separate the middle legs from the longitudinal axis, the middle leg will be placed a distance equal to corner legs plus the new distance d . Moreover, the width of the body is changed to 100mm. This is because, as we will see later, the algorithm gives us a d big enough to place in the middle of the body the microprocessor with enough space. See Table 4.

The results show an improvement for both stability margins if we move the placement of the middle legs. However, the algorithm gives us results that change our design considerably for both widths. This is, for example, that for an angle of 30° we will have a body that transforms in a new one which has a bigger width than the length. **A priori the best design is the one which offset in the corner legs is 45° with a width of 100mm.**

2.2.6. Design of the leg disposition and step length

As we have seen before, if we design the body in order to have an offset angle in the corner legs, we will need that the leg could be able to extend the distance necessary to place the foot in the next footstep. Different design of leg configuration have been discussed by different authors, but the most common configuration set in legged robots is the spider-like configuration (Fig. 19). This disposition gives the robot a sufficient walking speed, low CG height, enough walking speed and high obstacle avoidance. Those are the reason why we will set another two spider-like configuration in order to figure out which of this three suits better for the prototype to be built.

We will run again the algorithm for another 2 designs of legs in which the projection changes to 100mm and 120mm. In Table 5 and 6 we can see how does this affect to the stability margins and to the displacement of the middle legs. The distance d is reduced, while the stability margins are also

reduced. We will keep in mind those new designs of legs to see which is the best once every parameter is studied.

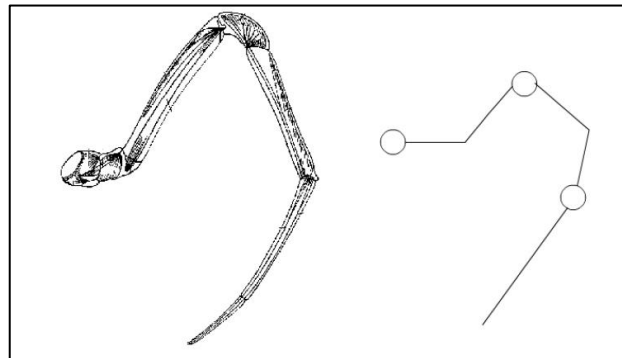


Figure 17. Aracnid type leg [43].

The next step will be setting the *step length*. We will have to consider a maximum angle between the tarsus articulation and the floor in order to avoid slippage. This will be set as 75 degrees, as we don't know the conditions of the terrain and the friction coefficient. The configuration of the leg placed in the ground with this angle will be called *safety configuration of the leg*.

We will calculate the *maximum step length* possible for each configuration, run the code again and see which of the design gives a high stability margins and a coherent geometric dimensions.

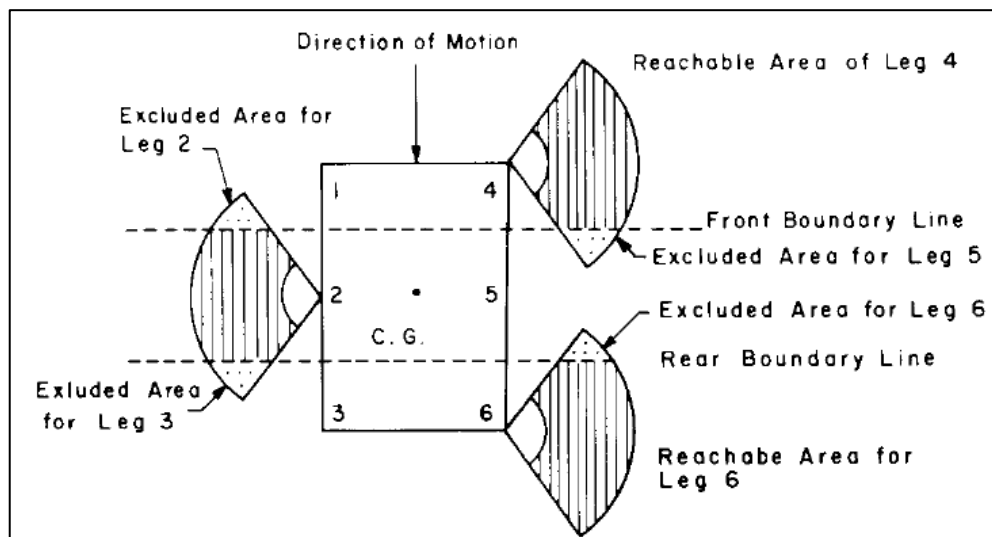


Figure 18. Reachable area of each leg [44].

The maximum step length will be defined by the parameter P_x , what we already know that is the distance between the centers of workspaces of the adjacent legs in one side. This is derivated from the



geometry of the robot, in which each leg has a reachable area in the form of a sector of an annulus (see Fig. 20). Since overlapping reachable areas raise interference problems, one way to solve it is to avoid it altogether by eliminating all overlapping reachable areas so that each leg has a distinct region that can be accessed only by it and not by any other leg. Moreover, for simplicity of analysis, we define a rectangular region as a reachable region of each leg. As we said before, the length of this rectangle will be determined by P_x . Nevertheless, we will set a length for the rectangle of each leg 19 mm smaller than P_x , having a dimension of 90mm ($P_x=109$ mm) for safety.

We will also have to consider that if this distance is bigger than the safety configuration of the leg, the maximum step length will be given by the distance that the foot is able to be positioned without being beyond the safety position of the leg. Knowing the safety configuration of the leg (the maximum angle with the floor) it is easy to get the projection of the leg in the plane XY by trigonometry:

- For the leg 1 (134mm), the safety configuration has a projection of160 mm.
- For the leg 2 (120mm), the safety configuration has a projection of146 mm.
- For the leg 3 (100mm), the safety configuration has a projection of146 mm.

Now that the maximum step length is known, we will run again the code for each configuration. The width of the body is changed again due to a small distance between the middle legs to place the microprocessor. The results are shown in Table 7, 8, 9, 10, 11 and 12.

Table 3. Stability margins

<i>Lb=250; Dw=150; L=134; Rx=50</i>							
Coxa Offset Angle	0°	10°	15°	20°	30°	40°	45°
Stability margin	62.91	77.45	84.45	91.2	103.79	114.88	119.78
Longitudinal Stability margin	64.33	79.85	87.45	94.88	109	121.76	127.5

Table 4. Stability margins and *d*

<i>Lb=250; Dw=100; L=134; Rx=50</i>							
Coxa Offset Angle	0°	10°	15°	20°	30°	40°	45°
Stability margin	62.51	76.79	83.63	90.22	102.42	113.09	117.79
Longitudinal Stability margin	64.33	79.84	87.45	94.87	109	121.76	127.5
<i>d</i> optimum	81.01	96.25	102.19	107.26	115.34	121.31	123.67



Table 5. Stability margins and d

$L_b=250; D_w=100; L=100; R_x=50$							
Coxa Offset Angle	0°	10°	15°	20°	30°	40°	45°
Stability margin	61.65	71.95	76.88	81.62	90.40	98.08	101.46
Longitudinal Stability margin	64.33	75.91	81.59	87.13	97.67	107.18	111.47
d optimum	66.04	75.67	79.63	83.11	88.86	93.26	95.04

Table 6. Stability margins and d

$L_b=250; D_w=100; L=120; R_x=50$							
Coxa Offset Angle	0°	10°	15°	20°	30°	40°	45°
Stability margin	62.22	74.85	80.91	86.73	97.51	106.95	111.11
Longitudinal Stability margin	64.33	78.22	85.04	91.69	104.33	115.75	120.9
d optimum	74.85	87.66	92.75	97.16	104.28	109.61	111.74

Table 7. Stability margins, d and maximum step length

$D_w=150; L=100$										
Coxa Offset Angle	0°	5°	10°	15°	20°	25°	30°	35°	40°	45°
Stability margin	55.34	59.1	62.76	66.27	69.63	73.52	80.68	87.49	93.89	99.84
Longitudinal Stability margin	57.67	62.02	66.35	70.61	74.76	79.46	87.21	94.56	101.48	107.91
d optimum	21.59	19.9	18.46	17.24	16.19	18.71	37.57	55.51	72.38	88.06
Maximum step length (R_x)	90	98.71	107.365	115.88	124.2	128.23	112.75	98.03	84.19	71.33



Table 8. Stability margins, d and maximum step length

$D_w=100; L=100$										
Coxa Offset Angle	0°	5°	10°	15°	20°	25°	30°	35°	40°	45°
Stability margin	54.56	58.15	61.6	64.9	68.02	71.68	78.66	85.3	91.54	97.34
Longitudinal Stability margin	57.67	62.02	66.35	70.6	74.77	79.46	87.2	94.56	101.49	107.91
d optimum	18.51	17.05	15.83	14.78	13.88	16.04	32.21	47.58	62.04	75.48
Maximum step length (R_x)	90	98.71	107.36	115.88	124.2	128.23	112.75	98.04	84.19	71.33

Table 9. Stability margins, d and maximum step length

$D_w=150; L=100$										
Coxa Offset Angle	0°	5°	10°	15°	20°	25°	30°	35°	40°	45°
Stability margin	55.76	60.41	64.91	72.21	81.69	90.88	99.70	108.09	115.98	--
Longitudinal Stability margin	57.67	62.86	68.08	76.01	85.98	95.66	104.95	113.77	122.08	--
d optimum	24.05	21.83	19.99	36.37	66.77	96.22	124.48	151.36	176.65	--
Maximum step length (R_x)	90	100.46	110.84	104.21	84.24	64.89	46.32	28.66	12.05	0

Table 10. Stability margins, d and maximum step length

$D_w=100; L=120$										
Coxa Offset Angle	0°	5°	10°	15°	20°	25°	30°	35°	40°	45°
Stability margin	55.2	59.68	68.09	71.12	80.46	89.52	98.21	106.47	114.24	--
Longitudinal Stability margin	57.67	62.89	68.08	76.01	85.98	95.66	104.95	113.77	122.08	--
d optimum	20.97	19.03	17.43	31.71	58.21	83.88	108.52	131.95	154	--
Maximum step length (R_x)	90	100.46	110.84	104.21	84.24	64.9	46.32	28.66	12.05	0

Table 11. Stability margins, d and maximum step length

$D_w=150; L=134$										
Coxa Offset Angle	0°	5°	10°	15°	20°	25°	30°	35°	40°	45°
Stability margin	56.01	61.26	66.36	74.62	85.27	95.58	105.47	114.88	123.73	--
Longitudinal Stability margin	57.67	63.51	69.3	78.21	89.35	100.15	110.52	120.38	129.66	--
d optimum	25.78	23.15	21.02	40.63	76.21	110.69	143.78	175.26	204.86	--
Maximum step length (R_x)	90	101.68	113.27	105.49	83.19	61.59	40.86	21.14	2.59	0

Table 12. Stability margins, d and maximum step length

$D_w=100; L=134$										
Coxa Offset Angle	0°	5°	10°	15°	20°	25°	30°	35°	40°	45°
Stability margin	55.45	60.64	65.56	73.68	84.18	94.36	104.12	113.41	122.15	--
Longitudinal Stability margin	57.67	63.51	69.3	78.21	89.35	100.15	110.52	120.38	129.66	--
d optimum	22.7	20.38	18.5	35.77	67.1	97.45	126.58	154.29	180.35	--
Maximum step length (R_x)	90	101.68	113.27	105.49	83.19	61.59	40.86	21.14	2.59	0

2.3. Check static stability in transfer phase

In order to know whether the design is statically stable or not we will have to check that the projection of the center of gravity of the robot falls into the support polygon, as we already explained. In a straight line movement, the distance that the projection of the CG can be moved from the static position will be given by the Longitudinal Stability Margin. We know the maximum step length of each design, so we can say that:

- $\frac{P_x}{2} \geq LSM$ the design is Statically Unstable.
- $\frac{P_x}{2} < LSM$ the design is Statically Stable.

Checking every configuration previously done in Tables 7, 8, 9, 10, 11 and 12 we check that every design reflected is Statically Stable.

However, this is set for a straight line movement. If we wanted to be sure that in every movement the robot does this rule is confirmed, we will use the static stability checking procedure.

2.3.1. Static Stability Checking Procedure

Static stability checking procedure is implemented to preserve balance and avoid unexpected falls. There is a number of stability criteria for legged robots e.g. stability margin, tumble stability margin, gradient, stability margin, energy stability margin, etc. (Hirose et al. (2001)). There is also a criterion which takes into account the friction coefficient between robot's feet and the ground (Bretl and Lall (2008)). Although it allows to precisely define the support polygon it can't be used for motion planning. The procedure is iterative and the computation cost is high. Because of that a fast, basic stability criterion defined by McGhee and Iswandhi (1979) is used in the presented motion planning system to check the balance for every planned posture of the robot.

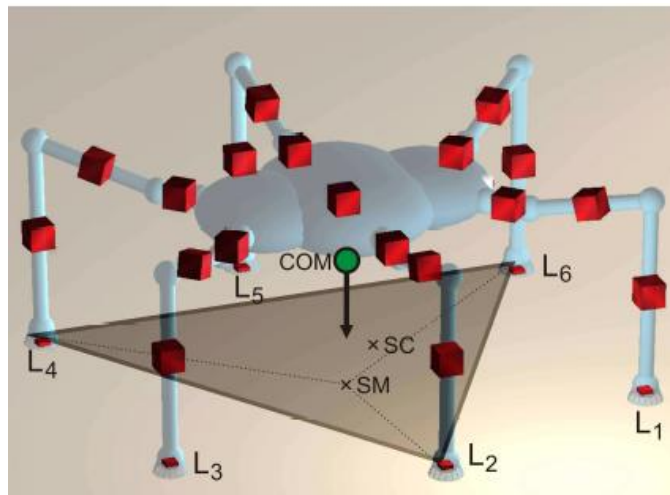


Figure 21. Projection of the CG in the support polygon [42].

The stability checking procedure is shown in the picture attached. At the beginning the centers of mass of all the robot's joints are computed. To compute the center of mass (COM) of the robot the instantaneous configuration of the legs and the trunk is used. The robot posture is taken into account during COM computation because a significant part of the robot's mass is allocated in the legs. Thus, a modification of the position of the legs significantly changes the COM position. Then a projection of the COM on the plane (SM) is computed. If the robot is statically stable, the SM point is located inside the convex hull formed by the contact points of the legs being in the stance phase. To check if the SM point is located inside the support polygon with L2, L4, L6 vertexes (an example for the tri-pod gait, cf. Fig. 3) the areas of the component triangles (4L2L4SM, 4L4L6SM, 4L6L2SM,) are computed. If the sum of areas equals the area of the support polygon, the SM point is inside the support polygon, and the robot is statically stable. If the sum of the areas is bigger than the area of the support polygon the SM point is outside the support polygon and the robot is not statically stable. This static stability



checking procedure is fast but approximate. In practice, to avoid risky postures, the area of the support polygon is reduced by relocating the leg contact points towards the center of the support polygon.

2.4. Model to be constructed

After analyzing all the valid models, we will have to get rid of those designs that don't reach the requirements specified. Those designs that have less than 100 mm of maximum step length are eliminated because they have a short range of mobility. Then, we set that the robot will have a normal step length of 50 mm. However, as it is an experimental robot, we will modify this parameter very often, so the R_x set to get the stability margins and the optimum d , will be the average between the normal step length and the maximum step length previously acquired. Having all these facts in mind, we will have to choose a model that tries to maximize the stability and that gives us the maximum R_x range possible. The model to be constructed, the one bold in green in Table 8, will have the following specifications:

Table 13. Model to be constructed

Length (Lb)	Width (Dw)	d	R_x typical	R_x optimum	R_x max	Offset Coxa Angle	P_x	Leg Projection	Stability Margin	Longitudinal Stability Margin
250 mm	100 mm	45 mm	50 mm	87.1 mm	124.2	20°	109 mm	100mm	74.76	80.95

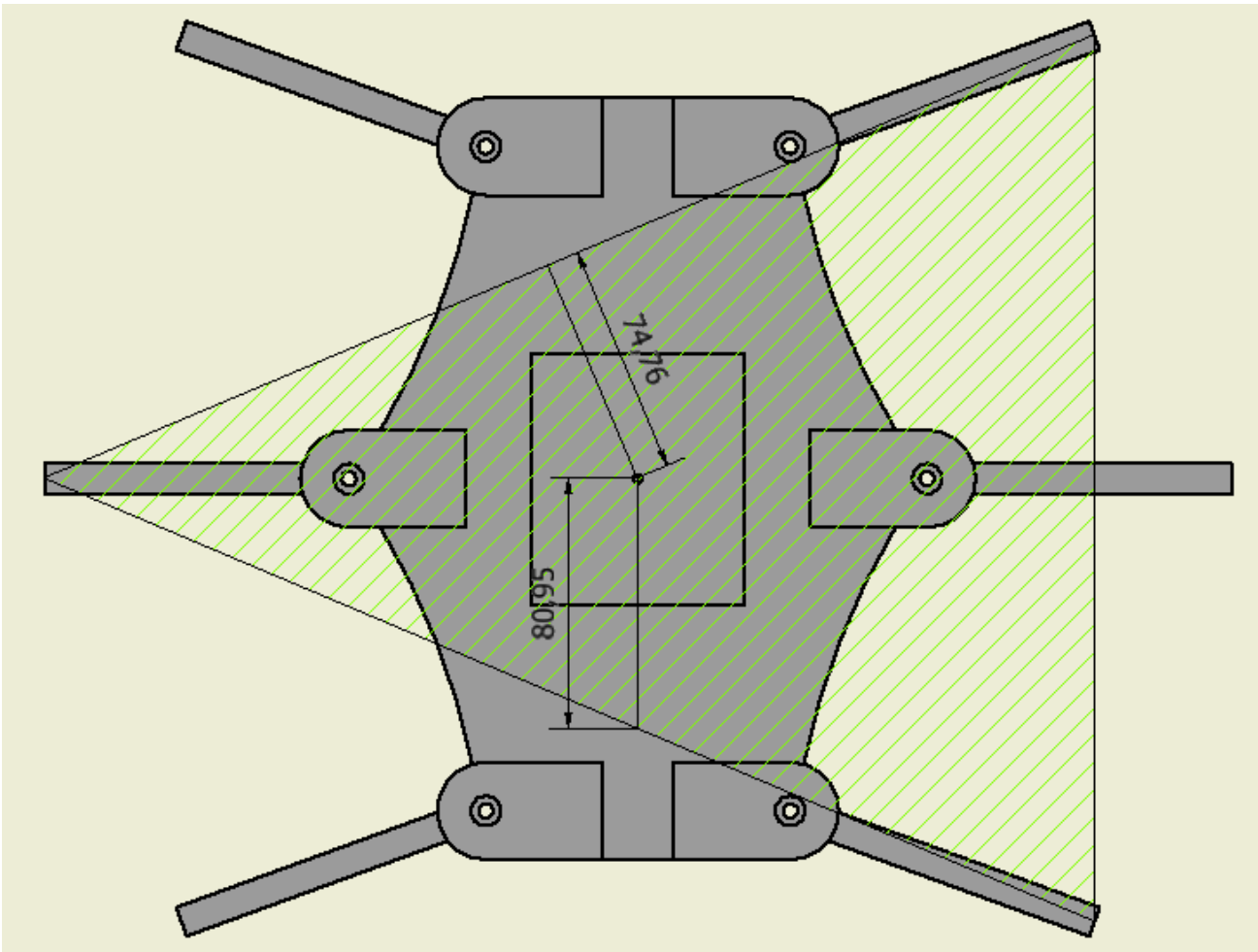


Figure 22. Static stability margin and Longitudinal Stability margin

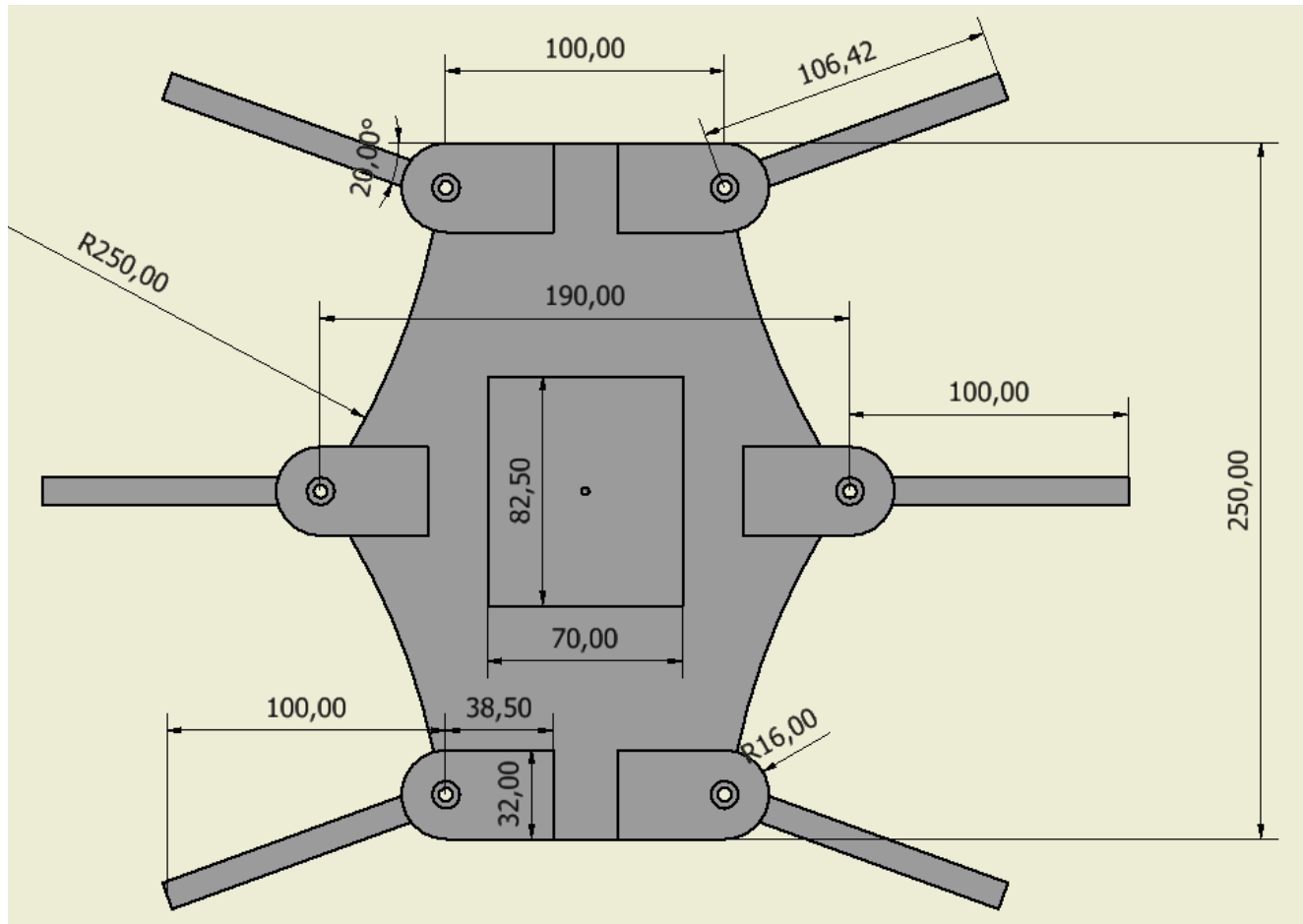


Figure 23. Dimensions of the prototype to be constructed.

2.5. Dynamic stability

2.5.1. Improving dynamic stability with body tilt, y-sway and e-sway

It is clear that dynamic stability is directly related to the implementation of the gait used to move the robot. Many researches have been done in order to improve the stability margins and the behavior of the robot in different terrain conditions. For example, Tsukagoshi *et al.* (1996) proposed to use the intermittent crawl gait, which intermittently drives the body, to maintain the center of gravity always at the central part of the supporting-legs' triangle. Due to the discontinuous nature of this gait, the speed of the vehicle will be relatively slow. Chen (1996) also proposed to include a lateral motion into gait planning to deal with the deformation problem of vehicle body mechanical structure.

When we observe a crocodile walking, a body sway motion is combined with the forward motion such that greater stability is achieved. In [29], a similar gait, including body sway motion into motion planning without reducing the forward speed of the vehicle, is proposed to increase the stability

margin. This sway motion can be included into motion planning for walking on level terrain or climbing a sloped surface, to increase the stability margin. In order to effectively and fairly evaluate the capabilities for increasing the stability margin of various body sway motions, definitions of various stability margins are surveyed. The Longitudinal Stability Margin (LSM) (Song and Waldron, 1987) and Stability Margin (SM) (Song and Waldron, 1987) are very useful for evaluating the stability of legged locomotion over relatively level terrain. However, because LSM and SM cannot provide a quantitative measure of stability when a multilegged vehicle walks on sloped terrain, Messuri and Klein (1985) proposed the definition of the Energy Stability Margin (ESM). ESM gives a quantitative measure of the impact energy that can be sustained by the vehicle without overturn.

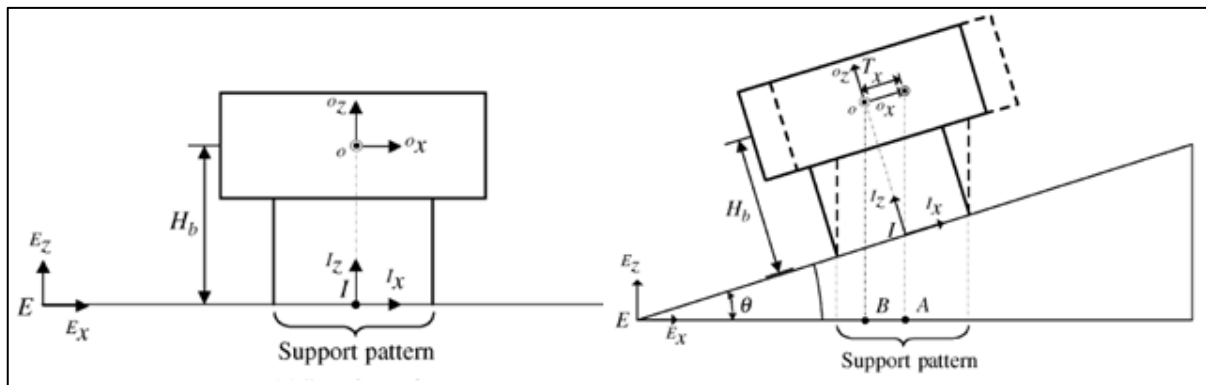


Figure 24. On the left robot on even terrain, on the right robot on sloped terrain [29].

Body-tilt compensation (Lee and Orin, 1988), for improving the stability margin when walking on sloped terrain, is also studied in this research. Further, two body sway motions: Y-Sway and E-Sway are proposed. The Y-Sway motion simply drives the y -component of the center of gravity (CG) of the vehicle to reach the y -component of the geometric center of the contact points of the supporting legs. The ESway motion, on the other hand, drives the y -component of the CG to reach the locus of the desired CG loci for considering equal Energy Stability Levels, defined in (Messuri and Klein, 1985).

In this article [29], there is a detailed demonstration on how the Energy Stability Margin is calculated. We will skip this for simplicity. There is also a demonstration on how does the body tilt, Y-sway and E-sway affect to the stability margin. The conclusions are very interesting and should be borne in mind for the future gait planning of our hexapod robot.

2.5.2. Body tilt

There are three possible cases to be distinguished in terms of body tilt. First, the robot is on a level terrain, the robot is on a sloped terrain with an inclination in the y axis, and the robot is on a sloped terrain with an inclination in both y and x axis.

In the three different cases we will have to move the body of the robot so that the projection of the center of gravity will coincide with the center of the support pattern. The body should be moved

parallel to the surface in order to maintain the original height. By doing this, we will maximize the stability margin.

This body motion for tilt compensation shall be considered in the initialization phase. The body only adjusts once to the slope before the robot starts walking.

2.5.3. Y-Sway Motion

In order to maintain the stability of the body, we simply drive the y-component of the CG to be equal to the y-component of the geometric center of the triangle formed by the contact points of the support pattern, which is the projection of the support boundary. However, for a hexapod robot moving in a straight line with tripod gait, the component y of the CG and the one of the geometric center will be the same.

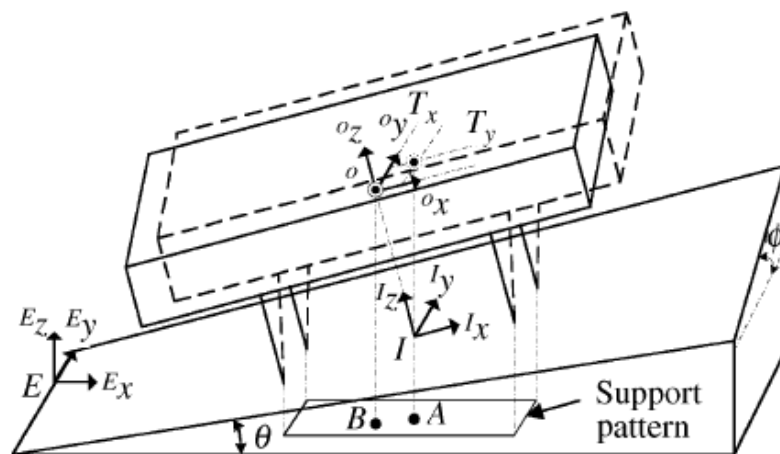


Figure 25. Robot on general sloped terrain [29].

2.5.4. E-Sway Motion

The way of further improve stability is by the implementation of E-Sway motion, which considers the CG locus for equal Energy Stability Levels.

This CG locus is the curve line which represents the location of the CG which has the maximum energy stability margin. This is defined as the geometric place for the CG where the Energy Stability Level of every edge of the Support Boundary is the same. And last, the Energy stability Level associated with a particular edge of the Support Boundary is equal to the work required to rotate the body CG, about that edge, to the position where the vertical projection of the body CG lies along the edge of the Support Boundary.



In this article we previously mention [29], a simulation with a quadruped robot is exposed. There are three cases, varying the sloped terrain as we saw for the body tilt compensation (Fig. 24 and 25). The simulation evaluates every three cases with and without Body tilt compensation, y-sway motion and e-sway motion. The results show that the stability improves with the Body tilt compensation, and we can conclude that Y-Sway is easy to implement and can obtain reasonably stable results, while E-sway is slightly involved but can obtain the best stability results. Nevertheless, both computational algorithms are simple enough so that they can be included into motion planning on real time.

Table 14. Maximum inclination angle with certified stability without slippage [29].

	Without body-tilt compensation	With body-tilt compensation (25 cm max)
No-sway	4°	22°
Y-sway	15°	32°
E-sway	24°	36°

(Without considering the foot-tip contact friction constraints.)



3. CONCLUSIONS

1. In this work the stability of the hexapod robot was observed. Results clearly show that the stability of the robot depends on the design of the body, legs distribution around the body, leg disposition, offset if coxa angle in corner legs, step length and the gaits.
2. The optimum leg disposition for maximizing static stability is arachnid type with a projection of 100mm on X-Y plane.
3. The optimum coxa angle for maximizing stability and step length is 20° in corner legs.
4. The maximum step length for maximizing stability and step length with safety conditions is 124.2 mm, with a typical step length of 87.1mm.
5. The optimum distance of displacement middle legs for maximizing stability and energy consumption for that leg disposition, coxa angle and step length is 45 mm.

4. REFERENCES

1. <http://es.wikipedia.org/wiki/Robot>
2. http://en.wikipedia.org/wiki/Autonomous_robot
3. Mahajan et al., 1997.
4. Bekker, 1960; Bekker, 1969
5. Kaneko, et al., 2002.
6. Yang and Kim, 1998; Hirose and Kato, 1998; Lee and Hirose, 2000; Yang, 2003; Spenneberg, et al., 2004
7. Nonami and Huang, 2001; Garcia, et al., 2003 or a tool (Ihme, 2003)
8. An Overview of Legged Robots J. A. Tenreiro Machado¹ and Manuel F. Silva
9. Design Issues for Hexapod Walking Robots Franco Tedeschi and Giuseppe Carbone
10. Lee, T.T.; Liao, C.M.; Chen, T.K. On the stability properties of hexapod tripod gait IEEE J. Robot. Autom. 1988, 4, 427–434.
11. Ding, X.; Wang, Z.; Rovetta, A.; Zhu, J.M. Locomotion analysis of hexapod robot. In Climbing and Walking Robots; In Tech: Rijeka, Croatia, 2010; pp. 291–310.
12. Preumont, A.; Alexadre, P.; Ghuys, D. Gait analysis and implementation of a six leg walking machine. In Proceedings of the Fifth International Conference on Advanced Robotics. Robots in Unstructured Environments (ICAR' 91), Pisa, Italy, 19–22 June 1991; Volume 2, pp. 941–945.
13. Takahashi, Y.; Arai, T. Development of multi-limb robot with omnidirectional manipulability and mobility. In Proceedings of the 2000 IEEE-RSJ International Conference on Intelligent Robots and Systems, Takamatsu, Japan, 31 October–5 November 2000; Volume 3, pp. 2012–2017.
14. Chu, S.K.-K.; Pang, G.K.-H. Comparison between different models of hexapod robot in fault-tolerant gait. IEEE Trans. Syst. Man Cybern. 2002, 32, 752–756.
15. Comparison between different model of hexapod robot in fault-tolerant gait Author(s) Chu, SKK; Pang, GKH
16. Stability analysis and synthesis of statically balanced walking for quadruped robots Freyr Hardarson
17. Silva, M.F.; Tenreiro Machado, J.A. A historical perspective of legged robots. J. Vib. Control 2007, 13, 1447–1486.
18. Delcomyn, F.; Nelson, M.E. Architectures for a biomimetic hexapod robot. Robot. Auton. Syst. 2000, 30, 5–15.
19. Billah, M.M.; Ahmed, M.; Farhana, S. Walking hexapod robot in disaster recovery developing algorithm for terrain negotiation and navigation. In New Advanced Technologies; Lazinica, A.; In Tech: Rijeka, Croatia, 2010.
20. Nava Rodríguez, N.E.; Carbone, G.; Ceccarelli, M.; Moreno Lorente, L.E. Design evolution of cassino hexapod robot. In Proceedings of the 10th Biennial ASME Conference on Engineering Systems Design and Analysis ESDA2010, Istanbul, Turkey, 12–14 July 2010.
21. Endo, G.; Hirose, S. Study on Roller-Walker: System integration and basic experiments. Robot. Autom. 1999, 3, 2032–2037.
22. Pfeiffer, F.; Eltze, J.; Weidemann, H. Six-legged technical walking considering biological principles. Robot. Autom. 1995, 14, 223–232.
23. Saranlı, U.; Buehler, M.; Koditschek, D.E. RHex—A simple and highly mobile hexapod robot. Int. J. Robot. Res. 2001, 20, 616–631.
24. Mechatronic systems and materials. Edited by Andrejus H. Marcinkevicius and Algirdas V. Valiulis. Trans Tech publications.



25. Zielinska, T. Autonomous walking machines, discussion of the prototyping problems. Bulletin of the Polish academy of sciences. Tech. Sci. 2010, 58, 443–451.
26. McGhee, R. B., and Frank, A. A. 1968. On the stability properties of quadruped creeping gaits. *Mathematical Biosciences* 3.
27. Shin-Min Song, Kenneth J. Waldron 1989. *Machines that walk: The adaptive suspension vehicle*
28. Kenneth S. Espenchied, Roger D. Quinn, Hillel J. Chiel, and Randall D. Beer. Leg coordination mechanisms in the stick insect applied to hexapod robot locomotion. volume 1, pages 455–468. *Adaptive Behavior*, 1993.
29. M. Hung, F. Cheng, H. Lee and D. E. Orin. Increasing the stability margin of multilegged vehicles through body sway.
30. S. Hirose, H. Tsukagoshi, K. Yoneda. Normalized Energy Stability Margin and its Contour of Walking Vehicles on Rough Terrain.
31. E. García P. Gonzalez de Santos. An Improved Energy Stability Margin for Walking Machines Subject to Dynamic Effects
32. Nava Rodríguez, N.E.; Carbone, G.; Ceccarelli, M.; Moreno Lorente, L.E. Design evolution of cassino hexapod robot. In *Proceedings of the 10th Biennial ASME Conference on Engineering Systems Design and Analysis ESDA2010, Istanbul, Turkey, 12–14 July 2010*.
33. *Journal of Bionic Engineering* 11 (2014) 176–187 Development of a Bionic Hexapod Robot for Walking on Unstructured Terrain He Zhang, Yubin Liu, Jie Zhao, Jie Chen, Jihong Yan.
34. P. Gonzalez de Santos, J. Estremera and E. García. Optimizing leg distribution around the body in hexapod robots.
35. Chu, SKK; Pang, GKH. Comparison between different model of hexapod robot in fault-tolerant gait. ©2002 IEEE.
36. <http://www.projectsodan.com/?tag=hexapod>
37. *Mechatronic systems and materials*. Edited by Andrejus H. Marcinkevicius and Algirdas V. Valiulis. Trans Tech publications.
38. Dynamixel AX-12 manual.
39. *Introduction to Autonomous Mobile Robots*. R Siegwart, IR Nourbakhsh, D Scaramuzza
40. Gaits and energetics in terrestrial legged locomotion D.C. Kar a,*, K. Kurien Issac b, K. Jayarajan a.
41. *Springer handbook of robotics*. Siciliano Khatib Editors.
42. Dominik Belter, Piotr Skrzypczynski. Integrated motion planning for a hexapod robot walking on rough terrain.
43. Dr. Nathir Rawashdeh. *Hexapod Robot, Robot design, model and control*
44. *IEEE JOURNAL OF ROBOTICS AND AUTOMATION*, VOL. 4. NO. 4. AUGUST
45. H. Zhang, Y. Liu, J. Chen, J. Yan. Development of a bionic Hexapod Robot for Walking on Unstructured Terrain.



ANNEX I

Code implemented in Mathematica to set the displacement of the middle legs:

```

In[188]:= (*-----FEATURES-----*)
(*-----BODY-----*)
Lb = 0.25; (*Length*)
Dw = 0.15; (*Width Front/Rear*)
Px = 0.109; (*Stroke Pitch*)
Mb = 0.5; (*Mass (kg)*)
H = 0.046; (*Height body*)
h = 0.03; (*Height leg*)
L = 0.1; (*Length leg (projection)*)
OffsetAngle = 25;
OffsetX = L * Sin[OffsetAngle Degree];
(*-----MAXIMUM STEPLENGTH-----*)
Print["MaxSL"]
MaxSL = (0.09 + OffsetX)
Print["MaxLeg"]
MaxLeg = Sqrt[(L)^2 + (MaxSL/2 + OffsetX)^2]
If [MaxLeg < 0.146, Rx = MaxSL,
    Rx = 2 * (Sqrt[(0.146)^2 - (L)^2] - OffsetX)];
Print["Rx"]
Rx (*Stroke (m)*)
(*-----LEG-----*)
L1 = 0.052; (*Length link 1(m)*)
L2 = 0.082; (*Length link 2(m)*)
L3 = 0.1; (*Length link 2(m)*)
Ml = 0.25; (*Mass (kg)*)

(*-----ROBOT-----*)
Mt = 2; (*Total mass (kg)*)
Pt = -9.8 * Mt;

(*-----ALGORITHM PARAMETERES-----*)
Nn = 20; (*Locomotion cycle(s)*)

(*-----BUCLE-----*)

(*-----EQUATIONS-----*)
x1[k_] := OffsetX + 1 * Px +
  ((-1)^(Floor[k/(Nn + 1)])) * Rx *
  (0.5 - (1/(Nn - 1)) * ((Mod[(k - 1), Nn] - 1)));
x2[k_] := OffsetX + 1 * Px +
  ((-1)^(Floor[k/(Nn + 1)])) * Rx *
  (0.5 - (1/(Nn - 1)) * ((Mod[(k - 1), Nn] - 1)));
x3[k_] :=
  0 * Px + ((-1)^(Floor[k/(Nn + 1)])) * Rx *
  (0.5 - (1/(Nn - 1)) * ((Mod[(k - 1), Nn] - 1)));

```



```

x4[k_] :=
  0 * Px + ((-1) ^ (Floor[k / (Nn + 1)])) * Rx *
  (0.5 - (1 / (Nn - 1)) * ((Mod[(k - 1), Nn] - 1)));
x5[k_] := -OffsetX - 1 * Px +
  ((-1) ^ (Floor[k / (Nn + 1)])) * Rx *
  (0.5 - (1 / (Nn - 1)) * ((Mod[(k - 1), Nn] - 1)));
x6[k_] := -OffsetX - 1 * Px +
  ((-1) ^ (Floor[k / (Nn + 1)])) * Rx *
  (0.5 - (1 / (Nn - 1)) * ((Mod[(k - 1), Nn] - 1)));

y1 = ((-1) ^ 2) * (Dw / 2 + L);
y2 = ((-1) ^ 3) * (Dw / 2 + L);
y3[d_] := ((-1) ^ 4) * (Dw / 2 + L + d);
y4[d_] := ((-1) ^ 5) * (Dw / 2 + L + d);
y5 = ((-1) ^ 6) * (Dw / 2 + L);
y6 = ((-1) ^ 7) * (Dw / 2 + L);

z1[k_] := h * (Sin[(Pi * k / Nn)]) * (1 - Floor[k / (Nn + 1)]) - H;
z2[k_] := -h * (Sin[(Pi * k / Nn)]) * (Floor[k / (Nn + 1)]) - H;
z3[k_] := -h * (Sin[(Pi * k / Nn)]) * (Floor[k / (Nn + 1)]) - H;
z4[k_] := h * (Sin[(Pi * k / Nn)]) * (1 - Floor[k / (Nn + 1)]) - H;
z5[k_] := h * (Sin[(Pi * k / Nn)]) * (1 - Floor[k / (Nn + 1)]) - H;
z6[k_] := -h * (Sin[(Pi * k / Nn)]) * (Floor[k / (Nn + 1)]) - H;

(*-----MATRIX-----*)
A1[k_, d_] :=  $\begin{pmatrix} x1[k] & x4[k] & x5[k] \\ y1 & y4[d] & y5 \\ 1 & 1 & 1 \end{pmatrix}$ ;
W1 =  $\begin{pmatrix} 0 \\ 0 \\ -Pt \end{pmatrix}$ ;
A12[k_, d_] := Inverse[A1[k, d]];
Mat1[k_, d_] := A12[k, d].W1;

F1[k_, d_] := (1 - Floor[k / (Nn + 1)]) * Mat1[k, d][[1, 1]];
F4[k_, d_] := (1 - Floor[k / (Nn + 1)]) * Mat1[k, d][[2, 1]];
F5[k_, d_] := (1 - Floor[k / (Nn + 1)]) * Mat1[k, d][[3, 1]];

A2[k_, d_] :=  $\begin{pmatrix} x2[k] & x3[k] & x6[k] \\ y2 & y3[d] & y6 \\ 1 & 1 & 1 \end{pmatrix}$ ;
A22[k_, d_] := Inverse[A2[k, d]];
Mat2[k_, d_] := A22[k, d].W1;

F2[k_, d_] := (Floor[k / (Nn + 1)]) * Mat2[k, d][[1, 1]];
F3[k_, d_] := (Floor[k / (Nn + 1)]) * Mat2[k, d][[2, 1]];
F6[k_, d_] := (Floor[k / (Nn + 1)]) * Mat2[k, d][[3, 1]];

(*-----RESULTS-----*)
Print["F1="]
F1d[k_] := F1[k, 0];
(*Plot[F1d[k], {k, 1, 40}]*)

Print["F3="]
F3d[k_] := F3[k, 0];
(*Plot[F3d[k], {k, 1, 40}]*)

Fi[d_] := F1[20.9999999, d] - F3[30, d];
(*we took the maximum observed in the previous plots*)

```



```
Print["Fi (d1="]
Fi[d]
Plot[Fi[d], {d, -3, 3}]
Print["Optimum d : for Fi(d)=0:"]
Solve[Fi[d] == 0, d]
dop = %[[1, 1, 2]]

(*-----GEOMERY CALCULATION-----*)
Print["LSM"]
LSM = ((Px + OffsetX) * (L + (Dw / 2) + dop)) / (2 * L + Dw + dop)
beta = N[ArcTan[(Px + OffsetX) / (2 * L + dop + Dw)] / Degree];
theta = 180 - beta - 90;
Print["SM"]
SM = LSM * Sin[theta Degree]
```

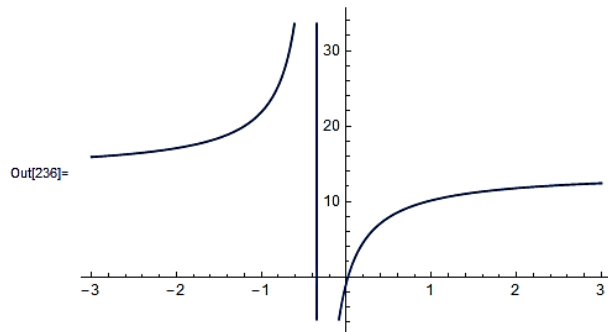
Example of results for the previous parameters:

```
MaxSL
Out[192]= 0.132262

MaxLeg
Out[194]= 0.147475

Rx
Out[197]= 0.12823

F1=
F3=
Fi (d1=
Out[235]= 0. +  $\frac{19.6 (-0.048911 - 0.215377 d)}{-0.105883 - 0.302524 d} - \frac{1.03766}{0.105883 + 0.302524 d}$ 
```



```
Optimum d : for Fi(d)=0:
Solve::ratnz :
Solve was unable to solve the system with inexact coefficients. The answer was obtained
by solving a corresponding exact system and numericizing the result. >>

Out[238]= {{d -> 0.0187143}}
Out[239]= 0.0187143

LSM
Out[241]= 0.0794696

SM
Out[245]= 0.0735232
```